

# Modeling apparent Pb loss in zircon U-Pb geochronology

Glenn R. Sharman<sup>1</sup>, Matthew A. Malkowski<sup>2</sup>

<sup>1</sup>Department of Geosciences, University of Arkansas, Fayetteville, AR 72701, USA

<sup>2</sup>Department of Geological Sciences, Jackson School of Geosciences, University of Texas at Austin, Austin, TX 78712, USA

Correspondence to: Glenn R. Sharman (gsharman@uark.edu)

**Abstract.** ~~Although-Because~~ the loss of radiogenic Pb from zircon is known to be a major factor that can cause inaccuracy in the U-Pb geochronological system, ~~there is a need to better characterize the~~ distribution of Pb loss in natural samples ~~has not been well characterized~~. Treatment of zircon by chemical abrasion (CA) has become standard practice in isotope dilution-thermal ionization mass spectrometry (ID-TIMS), but CA is much less commonly employed prior to *in-situ* analysis via laser ablation-inductively coupled plasma-mass spectrometry (LA-ICP-MS) or secondary ionization mass spectrometry (SIMS). Differentiating the effects of low levels of Pb loss in Phanerozoic zircon with relatively low precision *in-situ* U-Pb dates, where the degree of Pb loss is insufficient to cause discernible discordance, is challenging. We show that U-Pb isotopic ratios/dates that have been perturbed by Pb loss may be modeled by convolving a Gaussian distribution that represents random variations from the true isotopic value stemming from analytical uncertainty ~~the unperturbed U-Pb date distribution~~, with a distribution that characterizes Pb loss. We apply this mathematical framework to model the distribution of apparent Pb loss in 10 igneous samples that have both non-CA LA-ICP-MS or SIMS U-Pb dates and an estimate of the crystallization age, either through CA U-Pb or <sup>40</sup>Ar/<sup>39</sup>Ar geochronology. All but one sample showed negative age offsets that were unlikely to have been drawn from an unperturbed U-Pb date distribution. Modeling apparent Pb loss using the logit-normal distribution produced good fits with all 10 samples and showed ~~Because Pb loss is constrained to values between 100% and 0%, we suggest that the logit-normal distribution may be an appropriate~~. ~~Although the distribution type(s) that characterize Pb loss are not well known, we show that the logit normal distribution~~ Of the eight continuous distribution types we considered, modeling apparent Pb loss using the Weibull distribution produced, on average, the closest match with the non-CA U-Pb date distributions. We show two contrasting patterns in apparent Pb loss: samples where most zircon U-Pb dates undergo a bulk shift and samples where most zircon U-Pb dates exhibited low age offset but fewer grains/dates had more significant offset. Our modeling framework allows comparison of relative degrees of apparent Pb loss between samples of different age, with the first and second Wasserstein distances providing useful estimates of the total magnitude of apparent Pb loss. Given that the large majority of *in-situ* U-Pb dates are acquired without the CA treatment, this study highlights a pressing need for improved characterization of apparent Pb loss distributions in natural samples to aid in interpreting non-CA *in-situ* U-Pb data and to guide future data collection strategies.

## 30 1 Introduction

31 Zircon U-Pb geochronology is arguably one of the most important radiometric dating approaches used by geoscientists, with  
32 widespread application to constraining the age of Pleistocene and older geologic materials (Davis et al., 2003; Schoene, 2013;  
33 Gehrels, 2014). We rely on zircon U-Pb dates for calibrating the geological time scale (e.g., Compston, 2000a; 2000b; Bowring  
34 and Schmitz, 2003; Gradstein et al., 2004; Kaufmann, 2006), constraining the timing of important Earth history events (Froude  
35 et al., 1983; Schoene et al., 2010; 2015; Burgess et al., 2014), and determining the rates of Earth processes (Rioux et al., 2012;  
36 Schoene et al., 2012; Johnstone et al., 2019; Schoene et al., 2019). The zircon U-Pb geochronometer is particularly powerful  
37 due to the ability to assess agreement between the  $^{238}\text{U} \rightarrow ^{206}\text{Pb}$  and  $^{235}\text{U} \rightarrow ^{207}\text{Pb}$  decay chains, with  $^{206}\text{Pb}^*/^{238}\text{U}$  and  $^{207}\text{Pb}^*/^{235}\text{U}$   
38 dates in agreement plotting on the Concordia line, where \* indicates radiogenic Pb (Wetherill, 1956). ~~For example, a zircon  
39 that has undergone loss of radiogenic Pb will be pulled off the Concordia line towards the origin, thus becoming discordant  
40 (Fig. 1).~~

41

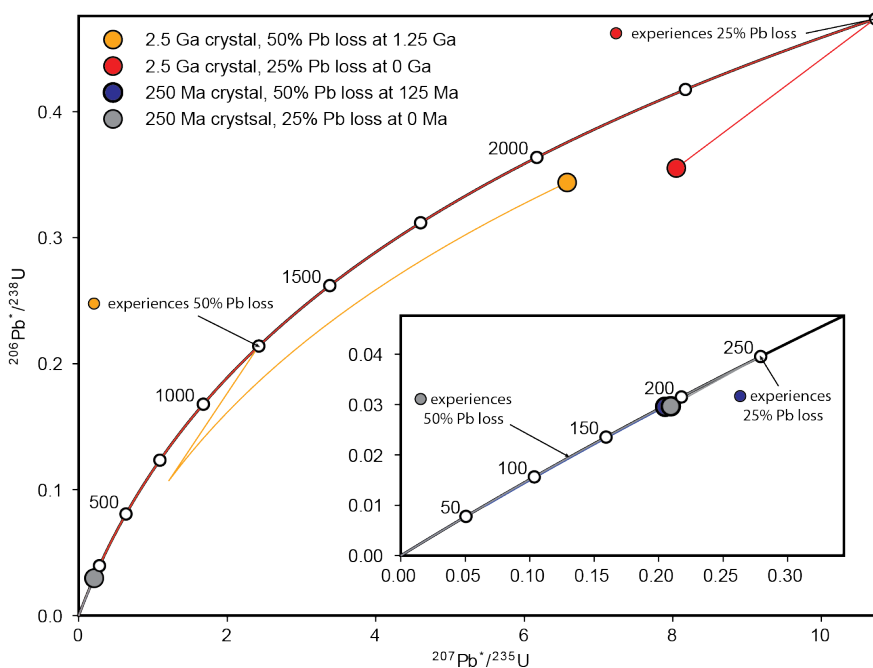


**Figure 1. Illustration of the influence of Pb loss on 250 Ma and 2.5 Ga zircon. Two Pb loss scenarios are shown: 25% loss at half the age of the zircon and 50% loss at present-day (0 Ma). The approximately linear nature of the  $^{206}\text{Pb}^*/^{238}\text{U}$  vs  $^{207}\text{Pb}^*/^{235}\text{U}$  Concordia line near the origin results in Pb loss producing limited discordance if the Pb loss occurs within several 100s of Myr of crystallization. Note that a greater amount of ancient Pb loss is required to produce the same shift in  $^{206}\text{Pb}^*/^{238}\text{U}$  relative to recent Pb loss. Thin, colored lines represent the path of each zircon.**

42

43

44 The causes and complications of open system behavior (e.g., radiogenic Pb loss) in zircon have long been a topic of ~~concern~~  
45 [study](#) (Tilton et al., 1955; [Pidgeon et al., 1966](#)). ~~Although Pb loss events may be discerned on U-Pb Concordia diagrams in~~  
46 ~~some circumstances and can provide useful geologic information about the thermal and/or fluid flow history of a region (Silver~~  
47 ~~and Deutsch, 1963; Blackburn et al., 2011; Morris et al., 2015; Kirkland et al., 2017),~~ with recognizing ~~and mitigating the~~  
48 ~~effects of Pb loss~~ ~~remaining~~ ~~remains~~ a ~~major~~ challenge ~~when it occurs within several 100's Myr of crystallization (Fig. 1;~~  
49 ~~Anderson et al., 2019).~~ For example, due to the shape of the  $^{206}\text{Pb}^*/^{238}\text{U}$  ~~versus~~  $^{207}\text{Pb}^*/^{235}\text{U}$  Concordia line, Pb loss ~~in~~  
50 ~~Phanerozoic zircon that occurs within several 100's Myr after crystallization~~ results in ~~discordance developing at a very low~~  
51 ~~angle relative to the Concordia line.~~ This ~~a~~ 'sliding along concordia' effect ~~that~~ can make Pb loss difficult to discern, particularly  
52 in relatively low-precision *in-situ* (i.e., LA-ICP-MS or SIMS) datasets when the Pb loss ~~only~~ produces ~~concordant or only~~  
53 ~~modestly discordance~~ ~~discordant analyses~~ (e.g., <10%; [Ashwal et al., 1999](#); Bowring and Schmitz, 2003; Ireland and Williams,  
54 2003; Reimink et al., 2016; Spencer et al., 2016; Watts et al., 2016; Anderson et al., 2019). Such low levels of Pb loss have  
55 been termed 'cryptic' and may be associated with spatial heterogeneities including radiation-damaged U-rich zones and  
56 microstructures (Nasdala et al., 2005; Kryza et al., 2012; Watts et al., 2016). Most Pb loss in zircon is likely a consequence of  
57 recrystallization or Pb transport in crystals with severe radiation damage ~~and exposure to hydrothermal alteration~~ (Silver and  
58 Deutsch, 1963; [Pidgeon et al., 1966](#); [Mezger and Krogstad, 1997](#); Cherniak and Watson, 2001; [Mezger and Krogstad, 2004](#);  
59 Marsellos and Garver, 2010). Mechanisms for Pb loss may include metamorphism (~~Kroner~~ [Kröner](#) et al., 1994; Orejana et al.,  
60 2015; Zeh et al., 2016), hydrothermal alteration (Geisler et al., 2002, 2003); diagenetic fluids or fluid flow (Willner et al.,  
61 2003; Morris et al., 2015; [Kirkland et al., 2020](#)), and chemical weathering (Stern et al., 1966; Black, 1987; Balan et al., 2001;  
62 Pidgeon et al., 2017; Andersen and Elburg, 2022). Pb loss is thought to primarily occur at temperatures <250°C in which  
63 radiation damage in zircon is unable to be annealed over geologic timescales (Schoene, 2013).

64  
65 Zircon domains that have lost Pb may be preferentially removed by first thermally annealing the zircon at high temperature  
66 (e.g., 800-1100°C) and then partially dissolving the zircon in a heated HF solution in a technique called chemical abrasion  
67 (CA) (Mattinson, 2005). The CA treatment is now routinely applied in ID-TIMS analysis and has contributed to both improved  
68 precision and accuracy of CA-ID-TIMS U-Pb data (Schoene, 2013). Although some *in-situ* U-Pb laboratories practice thermal  
69 annealing routinely (e.g., Allen and Campbell, 2012; Solari et al., 2015), CA has been applied much less frequently (Crowley  
70 et al., 2014; von Quadt et al., 2014; Watts et al., 2016; Ver Hoeve et al., 2018; Ruiz et al., 2022). Several studies that have  
71 conducted paired analysis of non-CA and CA of the same samples via *in-situ* U-Pb geochronology have found the non-CA U-  
72 Pb dates to skew younger than the CA U-Pb dates (Crowley et al., 2014; von Quadt et al., 2014; Watts et al., 2016). A growing  
73 number of maximum depositional age studies with tandem non-CA LA-ICP-MS and CA-ID-TIMS dating have shown the  
74 youngest non-CA U-Pb dates ~~tend to be younger than expected to skew young~~ relative to CA U-Pb dates or other geologic  
75 constraints, even when considering measurement uncertainty (e.g., Herriott et al., 2019; Schwartz et al., 2022; Howard et al.,  
76 2022; [Sharman et al., 2023](#)). However, there is a lack of quantitative constraints on the relative importance of Pb loss in

77 influencing non-CA U-Pb date distributions acquired via *in-situ* mass spectrometry, particularly as related to influencing  
78 depositional age constraints (Copeland, 2020).

79

80 This study builds upon past research on open system behavior in zircon by presents-presenting a novel-mathematical framework  
81 for quantifying the effects characterizing the distribution of apparent Pb loss on untreated (i.e., non-CA) U-Pb date distributions.  
82 We first suggest that U-Pb isotopic ratios that have been loss-perturbed by Pb loss U-Pb date distributions, or age offsets, may  
83 be viewed as the convolution of two signals: a Gaussian distribution that reflects measurement uncertainty about the true  
84 isotopic ratio the unperturbed U-Pb date distribution—and the distribution that characterizes Pb loss. We then apply this  
85 mathematical framework to model the distribution of apparent Pb loss that has affected 10 igneous samples of Miocene to  
86 Carboniferous age. Our results highlight the importance of quantifying distributions of apparent Pb loss magnitude -to better  
87 understand the potential influence on non-CA zircon U-Pb date distributions, s, with a need for improved characterization of  
88 to better resolve both the distribution types and magnitudes associated with Pb loss in zircon.

89

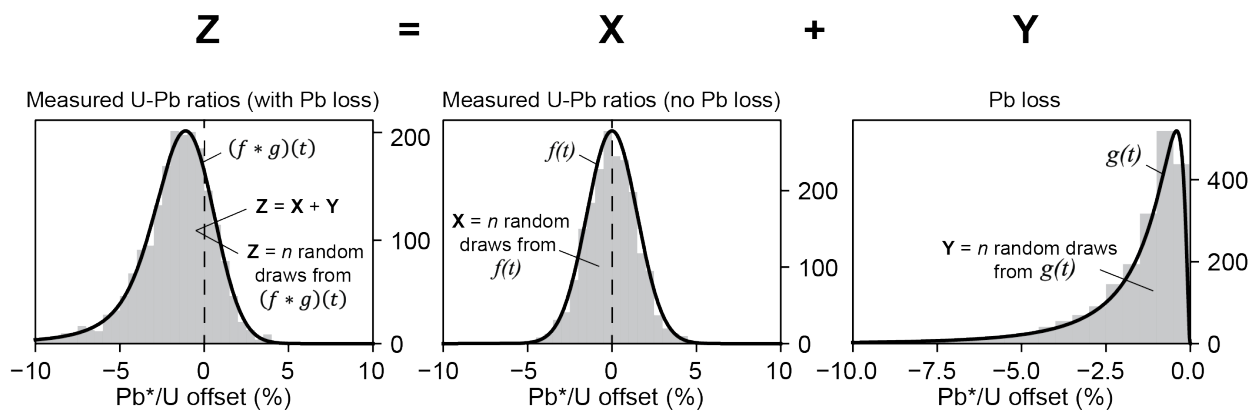


Figure 2. Illustration of how Pb\*/U isotopic ratios from  $n$  zircon analyses that have been perturbed by Pb loss ( $Z$ ) may be modeled as the summation of  $n$  non-perturbed Pb\*/U ratios ( $X$ ) and the amount of Pb loss encountered by each ( $Y$ ).  $X$  is drawn from  $f(t)$  that reflects the Gaussian distribution of Pb\*/U ratios that are unperturbed by Pb loss and  $Y$  is drawn from  $g(t)$  that represents the distribution of Pb loss in the sample. The distribution that characterizes  $Z$  may be found by convolving  $f(t)$  and  $g(t)$ . Although we assume that  $f(t)$  is a Gaussian distribution, the distribution type of Pb loss,  $g(t)$ , shown in this example as a logit-normal distribution ( $\mu=-4.5$ ,  $\sigma=1.0$ ) could take a number of discrete or continuous forms (Fig. 3). Note that in our modeling framework, values of  $X$ ,  $Y$ , and  $Z$  are normalized as percentage deviation from the true isotopic ratio (i.e., the mean of  $f(t)$ ), where negative values indicate that measured Pb\*/U is lower than the true ratio. See Supplemental Video 1 for an animation that illustrates the process of convolution and Supplemental Video 2 for an exploration of the logit-normal distribution in  $\mu$  and  $\sigma$  parameter space.

## 90 2 Mathematical framework

91 A series of  $n$  measurements of Pb loss-perturbed U-Pb\*/U measurements that have undergone Pb loss dates, Z, may be  
92 modeled as the sum of the corresponding unperturbed Pb\*/U U-Pb values dates, X, and the amount of that Pb\*/U changed due  
93 to Pb loss encountered by each date Pb loss for each date, Y,

94

$$Z = X + Y \quad (\text{Equation 1})$$

95

where  $Z$ ,  $X$ , and  $Y$  are all 1-D matrices with  $n$  values and [units of percentage offset from the true isotopic value](#) (Fig. 24).

96

Because Pb loss produces a lower [Pb\\*/UU-Pb ratio](#), the values of  $Y$  must be negative in our formulation of Equation 1

97

(Fig. 1). [If  \$X\$  is drawn from a Gaussian distribution  \$f\(t\)\$  whose mean \( \$\mu\$ \) approximates the true isotopic](#)

98

[value and whose standard deviation \( \$\sigma\$ \) reflects dispersion from the true value related to measurement uncertainty \(e.g.,](#)

99

[Schoene et al., 2013\) and if  \$Y\$  is drawn from a distribution that reflects Pb loss,  \$g\(t\)\$ , the U-Pb measurements unperturbed](#)

00

[by Pb loss \( \$X\$ \) have a shared true isotopic value,  \$\mu\$ , and that the unperturbed U-Pb ratios \( \$X\$ \) from cogenetic zircon may](#)

01

[be characterized by a Gaussian distribution,  \$f\(t\)\$ , whose mean \( \$\mu\$ \) equals the crystallization age and standard deviation \( \$\sigma\$ \)](#)

02

[reflects the degree to which the values of  \$X\$  deviate from the shared crystallization age. If these U-Pb ratios are then](#)

03

[subjected to Pb loss \( \$Y\$ \) that is drawn from  \$g\(t\)\$ , and if  \$X\$  and  \$Y\$  are independent, then  \$Z\$  may be viewed as being drawn from](#)

04

the convolution of  $f(t)$  and  $g(t)$

05

$$(f * g)(t) = \int_{-\infty}^{\infty} f(\tau)g(t - \tau)d\tau \quad (\text{Equation 2})$$

06

[provided that  \$X\$  and  \$Y\$  are independent where  \$g\(t\)\$  is reflected about the y axis and shifted in  \$\tau\$  space](#) (Fig. 24; Supplemental

07

Video 1). [Convolution simply represents the summation of two random variables, in this case one related to analytical](#)

08

[precision \(i.e., random variation around the true isotopic value stemming from the measurement process\) and the other](#)

09

[related to the geologic process of Pb loss. We model Pb loss as percentage offset from the true Pb\\*/U isotopic](#)

10

[ratio value crystallization age rather than deviation in absolute time \(i.e., Myr\) to promote comparison of samples of](#)

11

different age (Fig. 24).

12

13

[Because Pb loss is always negative and at most 100% of the crystallization age, we constrain  \$g\(t\)\$  is constrained to values](#)

14

[between 0% and 100%.](#)

15

$$g(t) = \begin{cases} 0\% & \text{if } g(t) > 0\% \\ -g(t) & \text{if } -100\% \leq g(t) \leq 0\% \\ -100\% & \text{if } g(t) \leq -100\% \end{cases}$$

16

17

Equation 2 may be solved analytically for some forms of  $f(t)$  and  $g(t)$ . For example, the convolution of Gaussian and

18

exponential distributions is known as the exponentially modified Gaussian distribution (Grushka, 1972; [Fig. 1; Supplemental](#)

19

[Video 1](#)). However,  $(f * g)(t)$  may also be solved numerically, which has the advantage of allowing both  $f(t)$  and  $g(t)$  to

20

take any form.

21

22

[Because Pb loss is always negative and at most 100% of the crystallization age,  \$g\(t\)\$  is constrained to values between 0%](#)

23

[and 100%. A sample where all zircon crystals undergo the same amount of Pb loss](#)

24

25

[Figure 32 illustrates the effects of both three discrete and continuous forms of  \$g\(t\)\$  on normally distributed U-Pb isotopic](#)

26

[ratios drawn from  \$f\(t\)\$ . A sample that experienced no Pb loss can be thought of as the convolution of  \$f\(t\)\$  with a discrete](#)

27

[form of  \$g\(t\)\$  where the 100% of probability corresponds to 0% Pb loss \(Fig. 32a\).](#)

28

29 Having 100% of probability for a discrete amount of Pb loss that is  $>0\%$  produces a bulk shift in the U-Pb age distribution  
 30 (i.e., constant Pb loss; Fig. 32b). Similarly, Pb loss experienced by only a subset of grains, or isolated Pb loss, may also be  
 31 modeled using a discrete distribution, (Fig. 32c). Alternatively, the Pb loss function  $g(t)$  could be represented by a  
 32 continuous probability distribution, where values of Pb loss vary continuously between values of 0% and 100% (Fig. 3d3).  
 33 Figure 3 illustrates the effects of eight different types of continuous distributions on modifying a Gaussian distribution  
 34 following convolution.

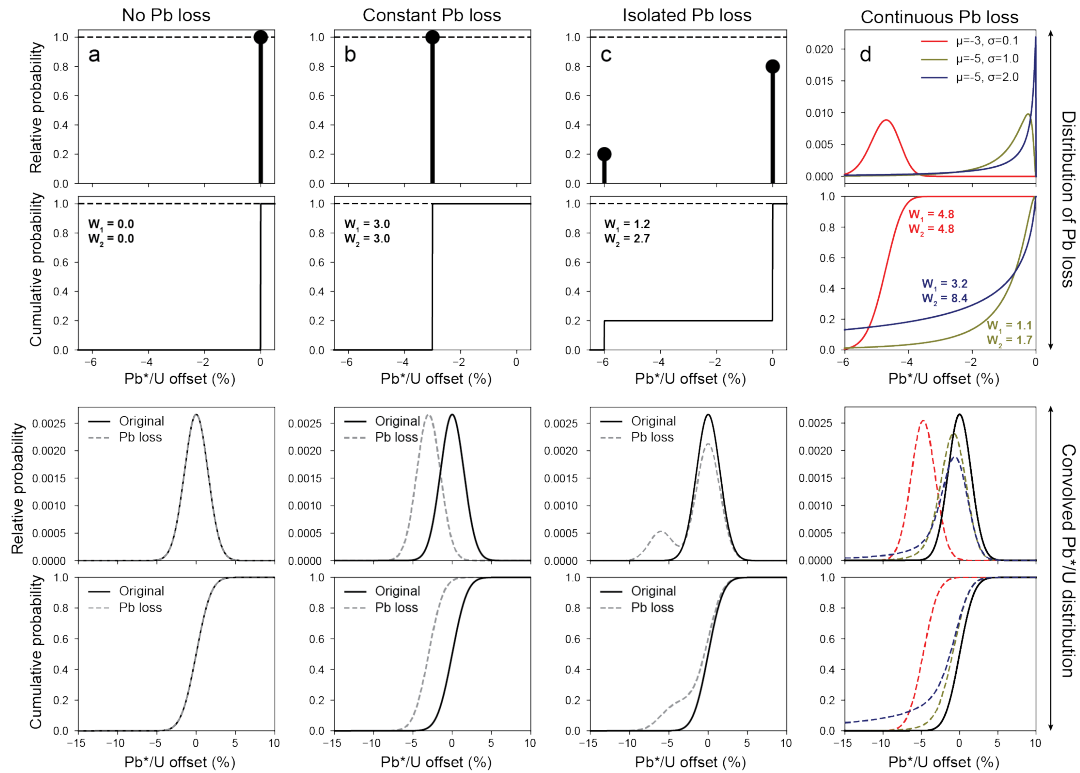


Figure 3. Illustration of how normally distributed zircon Pb\*/U values may be perturbed by discrete (a-c) or continuous (d) distributions of Pb loss. The top row represents the distribution of Pb loss in the sample expressed as a percentage of the true isotopic ratio (e.g.,  $^{206}\text{Pb}^*/^{238}\text{U}$  or  $^{207}\text{Pb}^*/^{235}\text{U}$ ) at the time of Pb loss, where the height of the black bar and ball indicates the relative probability of the specified Pb\*/U offset. Three discrete scenarios are shown: a) no Pb loss, b) constant Pb loss, and c) isolated Pb loss. A logit-normal distribution is shown as an example of continuous Pb loss in d). Additional examples of continuous Pb loss distributions are shown in Figure A1. The bottom row shows both the relative (above) and cumulative (below) probabilities of the unperturbed (solid black line) and Pb loss-perturbed (dashed line) Pb\*/U distributions.

35

36

### 37 3 Methods

#### 38 3.1 Modeling approach

39 We use the mathematical framework described above to model both the distribution of apparent Pb loss,  $g(t)$ , experienced by  
40 a group of cogenetic grains-crystals and their unperturbed U-Pb date distribution,  $f(t)$ . ~~Because  $g(t)$  could represent any~~  
41 ~~geological or analytical process that introduces negative age offsets, we use the phrase “apparent Pb loss” when describing our~~  
42 ~~modeled estimates of  $g(t)$ . For instance, matrix-related systematic errors (Allen and Campbell, 2012), addition of U-Th during~~  
43 ~~weathering (Pigdeon et al., 2019), and even sample contamination from younger minerals could introduce negative age shifts~~  
44 ~~exclusive of loss of radiogenic Pb. It should also be noted that the distribution of “apparent Pb loss” will underestimate the~~  
45 ~~magnitude of the true Pb loss event in the case of ancient Pb loss. This point is illustrated in Fig. 1 where a 50% reduction in~~  
46  ~~$Pb^*$  at 125 Myr after crystallization produces a similar offset in  $^{206}Pb^*/^{238}U$  versus the same grain that lost 25% of its  $Pb^*$~~   
47 ~~at 250 Myr (present day). If~~ Because Pb loss is isotopically indiscriminate, Equation 2 may be equally applied to  $^{206}Pb^*/^{238}U$   
48 and  $^{207}Pb^*/^{235}U$ . However, we model  $^{206}Pb^*/^{238}U$  ratios as these have much lower analytical uncertainty for the Carboniferous  
49 and younger samples analyzed in this study.

50

51 To model  $g(t)$ , we allow the  $\mu$  of  $f(t)$  to vary within the 95% confidence interval associated with an independent estimate of  
52 the crystallization age. We then estimate both  $g(t)$  and  $\sigma$  of  $f(t)$  by iteratively solving for the combination of parameters that  
53 minimize the misfit between the measured  $Pb^*/U$ -~~Pb-dates~~values and the modeled distribution  $(f * g)(t)$  using the Python  
54 `scipy.optimize.minimize()` function. We define misfit as the sum of squared residuals between the empirical cumulative  
55 distribution function (ECDF) of the measured U-Pb-dates $Pb^*/U$  values and the cumulative density function (CDF) of the  
56 modeled-U-Pb-age  $Pb^*/U$  distribution. ~~In total, we consider 11 different distribution types for  $g(t)$  that consist of both discrete~~  
57 ~~(no Pb loss, constant Pb loss, and isolated Pb loss; Fig. 2) and continuous (uniform, gamma, exponential, Rayleigh, Weibull,~~  
58 ~~Pareto, half normal, and lognormal; Fig. 3) distributions.~~

59

60 If both non-CA and CA analyses are available from the same sample, then the distribution of CA U-Pb dates may be used to  
61 constrain the parameters of  $f(t)$ . For such samples, we modify the approach described above by first finding the Gaussian  
62 distribution  $f(t)$  that most closely approximates the treated U-Pb-date $Pb^*/U$  distribution. We then use this best-fitting  $f(t)$  in  
63 estimating  $g(t)$  using the minimization-of-misfit technique described above. Such datasets have the advantage of providing  
64 constraints on  $\sigma$  of  $f(t)$ , which is otherwise treated as an unknown parameter during modeling if only non-CA U-Pb dates are  
65 available.

66

67 In order to estimate  $g(t)$  as described above, we must choose one or more reasonable parametric models that are appropriate  
68 for describing distributions of Pb loss. One possibility is that all zircon crystals in the sample experienced the same amount  
69 of Pb loss, which could shift  $Pb^*/U$  from 0% to -100% of its value ~~because Pb loss is always negative and at most -100%.~~  
70 Such a scenario of constant Pb loss may be modeled by a discrete form of  $g(t)$  where a single parameter specifies the  
71 percentage of Pb lost (~~<0% and >100%~~). Convolution of such a discrete form of  $g(t)$  simply produces a negative shift in the  
72  $U-Pb/Pb^*/U$  values (i.e., Fig. 3b).

73  
74 Another possibility is that Pb loss was experienced by only a subset of ~~grains~~ crystals (i.e., isolated Pb loss). This scenario  
75 may also be modeled by assigning  $g(t)$  to a discrete distribution with two parameters: one that indicates the fraction of Pb  
76 lost (~~<0% and >100%~~) and one that specifies the proportion of ~~grains~~ crystals that underwent Pb loss (Fig. 3c). This  
77 parameterization of  $g(t)$  will produce a bimodal pattern in U-Pb values, particularly if the degree of Pb loss is significant  
78 relative to measurement uncertainty (Fig. 3c).

79  
80 Instead of modeling  $g(t)$  as a discrete distribution where Pb loss is restricted to certain values, we may also consider a  
81 continuous probability distribution where values of Pb loss can take on any value between 0% and -100% (Fig. 3d).  
82 ~~Because~~ Rather than assume ~~we do not know~~ a priori the form(s) that  $g(t)$  might take, we considered a wide range of 1- or 2-  
83 parameter distributions for the purposes of exploratory modeling (Appendix A). Of the distribution types considered, we  
84 identified the logit-normal distribution, also known as the logistic normal distribution, as perhaps the most reasonable for  
85 modeling Pb loss. The logit-normal distribution has the property of having a logit (i.e., the quantile function of the logistic  
86 distribution) that is normally distributed with a geometric mean of  $\mu$  and standard deviation of  $\sigma$  (Aitchison and Shen, 1980;  
87 Mead, 19654).

88 
$$f(x, \mu, \sigma) = \frac{1}{\sigma\sqrt{2\pi}} \frac{1}{x(1-x)} e^{-\frac{(\text{logit}(x)-\mu)^2}{2\sigma^2}} \quad \text{_____ (Equation 3)}$$



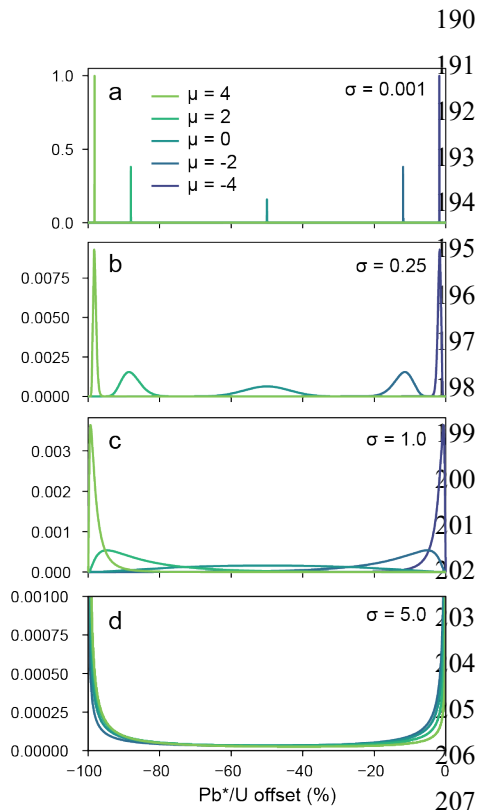


**Figure 4. Exploration of the logit-normal distribution's parameter space. Note that we have rescaled the x-axis of the logit-normal distribution such that  $-100 < x < 0$ .**

The logit-normal distribution is well-suited for modeling constrained data types (e.g., compositional data; Atchison and Bacon-Shone, 1999; Vermeesch, 2018b) in part due to it being defined over  $0 < x < 1$ . We invert and scale the distribution to extend from  $-100\% < x < 0\%$  to match the sign and units of Pb\*/U offset due to Pb loss when expressed as a percentage (Fig. 3d).

Figure 4 explores the relationship of the logit-normal distribution to its two parameters ( $\mu$  and  $\sigma$ ) (see also Supplemental Video 2). The distribution has a 'spiky' character when  $\sigma$  is a very small number (e.g., 0.001; Fig. 4a), which would be a reasonable approximation for samples that underwent an approximately constant amount of Pb loss (e.g., Figs. 3a and 3b). Although the logit-normal distribution cannot model 0% or 100% Pb loss, these values may be approximated by making  $\mu$  a large negative or positive number, respectively. A sample where most zircon exhibit very little Pb loss but with fewer zircon experiencing significant Pb loss could be produced by  $\mu = -4$  and  $\sigma = 1.0$  (Fig. 4c). Alternatively, a sample with a peak probability of Pb loss  $< 0\%$  may be modeled using moderate values of  $\sigma$  (e.g., 0.25-1; Figs. 4b and 4c). The logit-normal distribution produces bimodal distributions where most probability is close to 0% and -100% when  $\sigma$  values are high (e.g.,  $>> 1$ ; Fig. 4d).

12

### 13 3.2 Samples

14 We apply the mathematical and modeling framework presented above to estimate the distribution of apparent Pb loss in 10  
 15 igneous samples that range in age from Carboniferous to Miocene, nine of which have been published previously (Table 1).  
 16 Samples CTU, RCP, and SRF are all from upper Eocene rhyolites of the Caetano caldera system of the western United States  
 17 (Watts et al., 2016). These samples were split into non-CA and CA aliquots prior to analysis via SIMS (Watts et al., 2016).  
 18 We used the error-weighted mean age of the CA U-Pb dates as an estimate of the true crystallization age for each sample, with  
 19 weighted means approximately 0.4-0.6 Myr older than the corresponding  $^{40}\text{Ar}/^{39}\text{Ar}$  sanidine ages (Watts et al., 2016). The  
 20 number of analyses per aliquot (non-CA or CA) ranges from 17-34 for these three samples (Table 1).

**Table 1. Sample Summary**

Sample	Age (Ma)	Reference	N (non- CA)	N (CA)	Model results (best fit logit-normal distribution)					
					$f(t)$ (Ma)	$g(t)$ sum of squared residuals	$g(t)$ parameters	$g(t)$ P2.5-P50- P97.5 (%)	$W_1$	$W_2$
ELM18 DVTC- 10	15.7 $\pm 0.2$ ( $2\sigma$ ) <sup>1</sup>	Miller et al. (2022)	144	n.a.	15.90 $\pm$ 0.55 ( $1\sigma$ )	1.0	$\mu = -3.24$ $\sigma = 1.28$	-32.49 -3.77 -0.32	6.9	11.1
248-2	24.422 $\pm 0.25$ ( $2\sigma$ ) <sup>3</sup>	von Quadt et al. (2014)	30	55	24.42 $\pm$ 0.64 ( $1\sigma$ )	2.7	$\mu = -4.48$ $\sigma = 1.06$	-8.3 -1.12 -0.14	1.9	3.0
029-5 <sup>5</sup>	24.480 $\pm 0.084$ ( $2\sigma$ ) <sup>3</sup>	von Quadt et al. (2014)	42	48	24.47 $\pm$ 0.79 ( $1\sigma$ )	3.3	$\mu = -3.10$ $\sigma = 0.47$	-10.17 -4.31 -1.76	4.7	5.2
059-1 <sup>5</sup>	24.57 $\pm 0.28$ ( $2\sigma$ ) <sup>2</sup>	von Quadt et al. (2014)	41	36	24.50 $\pm$ 0.95 ( $1\sigma$ )	1.1	$\mu = -3.48$ $\sigma = 0.52$	-7.87 -2.99 -1.1	3.4	3.8
CTU	34.41 $\pm 0.26$ ( $2\sigma$ ) <sup>2</sup>	Watts et al. (2016)	24	18	34.47 $\pm$ 0.83 ( $1\sigma$ )	2.1	$\mu = -3.21$ $\sigma = 0.29$	-6.65 -3.88 -2.23	4.0	4.2
RCP	34.38 $\pm 0.32$ ( $2\sigma$ ) <sup>2</sup>	Watts et al. (2016)	34	18	34.19 $\pm$ 0.75 ( $1\sigma$ )	3.1	$\mu = -3.96$ $\sigma = 0.80$	-8.38 -1.87 -0.40	2.5	3.3
SRF	34.62 $\pm 0.37$ ( $2\sigma$ ) <sup>2</sup>	Watts et al. (2016)	17	17	34.25 $\pm$ 0.75 ( $1\sigma$ )	5.1	$\mu = -4.57$ $\sigma = 1.08$	-7.92 -1.03 -0.12	1.8	2.9
DG 026	76.41 $\pm 0.45$ ( $2\sigma$ ) <sup>3</sup>	von Quadt et al. (2014)	31	34	76.16 $\pm$ 1.42 ( $1\sigma$ )	3.0	$\mu = -3.74$ $\sigma = 0.56$	-6.65 -2.32 -0.79	2.7	3.1
MM20- EC- 109 <sup>6</sup>	144.50 $\pm 0.07$ ( $2\sigma$ ) <sup>4</sup>	This study	68	n.a.	144.43 $\pm$ 3.12 ( $1\sigma$ )	1.6	$\mu = -4.73$ $\sigma = 1.91$	-27.16 -0.87 -0.02	3.6	8.8
AvQ 244 <sup>7</sup>	333.60 $\pm 0.66$ ( $2\sigma$ ) <sup>3</sup>	von Quadt et al. (2014)	17	19	333.64 $\pm$ 10.86 ( $1\sigma$ )	12.3	$\mu = -2.69$ $\sigma = 0.82$	-25.30 -6.36 -1.34	8.1	10.3

- 22  
23 <sup>1</sup>Sanidine <sup>39</sup>Ar/<sup>40</sup>Ar age (Snow and Lux, 1999)  
24 <sup>2</sup>Error-weighted mean of chemically abraded U-Pb dates  
25 <sup>3</sup>Concordia age (CA-ID-TIMS)  
26 <sup>4</sup>Error-weighted mean 5 of 5 zircon crystals analyzed via CA-ID-TIMS  
27 <sup>5</sup>U-Pb dates older than 28 Ma excluded from analysis  
28 <sup>6</sup>U-Pb dates older than 158 Ma excluded from analysis  
29 <sup>7</sup>U-Pb dates older than 360 Ma excluded from analysis  
30 N = Number of analyses  
31 n.a. = Not available  
32  $W_1$  = first Wasserstein distance  
33  $W_2$  = second Wasserstein distance  
34  
35

36 We present analysis of five samples reported in von Quadt et al. (2014), including upper Oligocene andesite/trachy-andesite  
37 from Macedonia (248-2, 029-5, and 059-1), upper Cretaceous dolerite from Romania (DG\_026), and middle Carboniferous  
38 granite from West-Bulgaria (AvQ 244). These samples were also split into non-CA and CA aliquots prior to analysis via LA-  
39 ICP-MS. For samples other than 059-1 we use concordia ages from CA-ID-TIMS analyses of between three and six crystals  
40 for the crystallization age of each sample (von Quadt et al., 2014; Table 1). For sample 059-1 we used the weighted mean of  
41 the CA U-Pb dates. The number of analyses per sample (non-CA or CA) ranged from 17-55 for this dataset (Table 1).

42  
43 Sample ELM18DVTC-10 is from a Miocene ash-flow tuff from the Pangua Formation in the western United States that has  
44 144 U-Pb dates acquired via LA-ICP-MS (Miller et al., 2022). We use a  $^{40}\text{Ar}/^{39}\text{Ar}$  weighted mean age of  $15.7 \pm 0.2$  Ma ( $2\sigma$ )  
45 from the same unit as an estimate of the crystallization age of this sample (sample 592-GV1 of Snow and Lux, 1999). Sample  
46 ELM18DVTC-10 was highlighted by Schwartz et al. (2022) who noted the youngest zircon U-Pb dates to be much younger  
47 than the accepted  $^{40}\text{Ar}/^{39}\text{Ar}$  age of this unit. Miller et al. (2022) also noted the presence of these young [grains-zircon](#) and  
48 suggested that they may be a consequence of surface contamination from units higher in the section.

49  
50 Sample MM20-EC-109 is a Lower Cretaceous intermediate ash interbedded within marine carbonaceous mudstone from the  
51 Rio Mayer Formation of Argentina with 68 zircon U-Pb dates acquired via LA-ICP-MS (Table A32). Laser ablation spot  
52 locations were selected on the rim and/or core of the [grain-zircon](#) guided by CL images (Figure A2A3), with 59 [grains-zircon](#)  
53 [crystals analyzed](#) in total ~~analyzed~~. We use a crystallization age of  $144.43 \pm 0.07$  Ma ( $2\sigma$ ) derived from a weighted mean  
54 [average](#) of five zircon crystals analyzed via CA-ID-TIMS at the Boise State University Isotope Geology Laboratory (Table  
55 A43). This sample exhibits a large offset between the youngest U-Pb dates acquired via LA-ICP-MS, up to ~60% younger  
56 than the CA-ID-TIMS weighted mean.

### 57 3.3 Statistical analysis

58 To evaluate the likelihood that the measured [Pb\\*/UU-Pb\\_date](#) distribution could have been drawn from the modeled  $(f * g)(t)$ ,  
59 we apply the nonparametric, 1-sided Kolmogorov-Smirnov (K-S) and Kuiper statistical tests that compare the ECDF  
60 with the cumulative CDF of  $(f * g)(t)$  (Press, 2007). The Kuiper statistic is relatively more sensitive in differences in the tails  
61 of the distributions versus the K-S statistic (Vermeesch, 2018a). We reject the null hypothesis that the non-CA U-Pb dates  
62 were drawn from  $(f * g)(t)$  if the K-S or Kuiper p-value is  $< 0.05$  (i.e., 95% confidence level). We thus interpret p-values  
63  $> 0.05$  to indicate that the non-CA U-Pb dates could have been plausibly drawn from  $(f * g)(t)$  at a 95% confidence level  
64 (Press, 2007). However, it should be noted that Saylor and Sundell (2016) found that both K-S and Kuiper p-values more  
65 frequently reject the null hypothesis than expected. We thus use p-values as a general guideline to model goodness-of-fit.

66

67 The Wasserstein distance has been recently proposed as a metric for quantifying the dissimilarity between detrital zircon U-  
68 Pb age distributions (Lipp and Vermeesch, [in review 2023](#)). We consider the first and second Wasserstein distances,  $W_1$  and  
69  $W_2$ , to be useful approximations for the total degree of negative  $\text{age-Pb}^*/\text{U}$  perturbation that a set of analyses has experienced,

$$70 \quad W_1 = \int_0^1 |M^{-1} - N^{-1}| dt \quad (\text{Equation 3})$$

$$71 \quad W_2 = \sqrt{\int_0^1 |M^{-1} - N^{-1}|^2 dt} \quad (\text{Equation 4})$$

72 where  $M^{-1}$  and  $N^{-1}$  are the inverses of the CDFs  $M$  and  $N$ . Because values of Pb loss are restricted to between ~~-100% and 0%~~  
73 [and 100%](#), both  $W_1$  and  $W_2$  yield maximum possible values of 100 (i.e., 100% of [grains-analyses](#) have -100%  $\text{age-Pb}^*/\text{U}$   
74 offset, or the U-Pb system is completely reset). The  $W_1$  simply equates to the area beneath the cumulative probability  
75 distribution of  ~~$g(t)$  the apparent Pb loss function~~ (e.g., Fig. 3). Because the  $W_2$  distance involves a squaring of the distance  
76 between the quantile functions, it imparts a higher cost penalty for the part of the distribution with strongly ~~negative~~-offset  
77 values. For example, the  $W_1$  and  $W_2$  distances are equal for a Pb loss function characterized by constant Pb loss (e.g., -3% Pb  
78 loss produces  $W_1$  and  $W_2$  values of 3, Fig. [3b2](#)). However, the  $W_2$  distance is often much larger than  $W_1$  for Pb loss  
79 distributions with a heavy tail, ~~such as the Pareto distribution~~ (Fig. [3d](#)). As such, the  $W_2/W_1$  ratio provides an approximation  
80 of Pb loss distribution asymmetry, with values of 1 indicating constant Pb loss and values  $\gg 1$  indicating highly asymmetric  
81 Pb loss.

82

#### 83 **4 Results**

84 ~~Figure X presents a summary of model misfit for each of the 10 samples and 4 primary distribution types considered (see~~  
85 ~~Appendix A for additional results).~~

86

87 ~~Of the four primary types of Pb loss distributions considered (Fig. 3), the logit-normal distribution yielded the lowest average~~  
88 ~~misfit with a value of 3.5, followed by the isolated Pb loss scenario (average of 4.5) and the constant Pb loss scenario (average~~  
89 ~~of 10.5) (Table A2; see also Appendix A). he no Pb loss scenario produced~~

90

91 ~~The isolated Pb loss scenario also produced the closest match with samples RCP, SRF, DG 026, and AvQ 244.~~

92

93 ~~isolated Pb loss yielded the lowest average misfit with a value 4.2 (Fig. 4). The scenario of no Pb loss, however, performed the~~  
94 ~~worst of any scenario that we considered, with an average misfit of 101.3497.4 (Table A2 Fig. 4). Correspondingly, both K-S~~  
95 ~~and Kuiper p-values for the no Pb loss~~

96

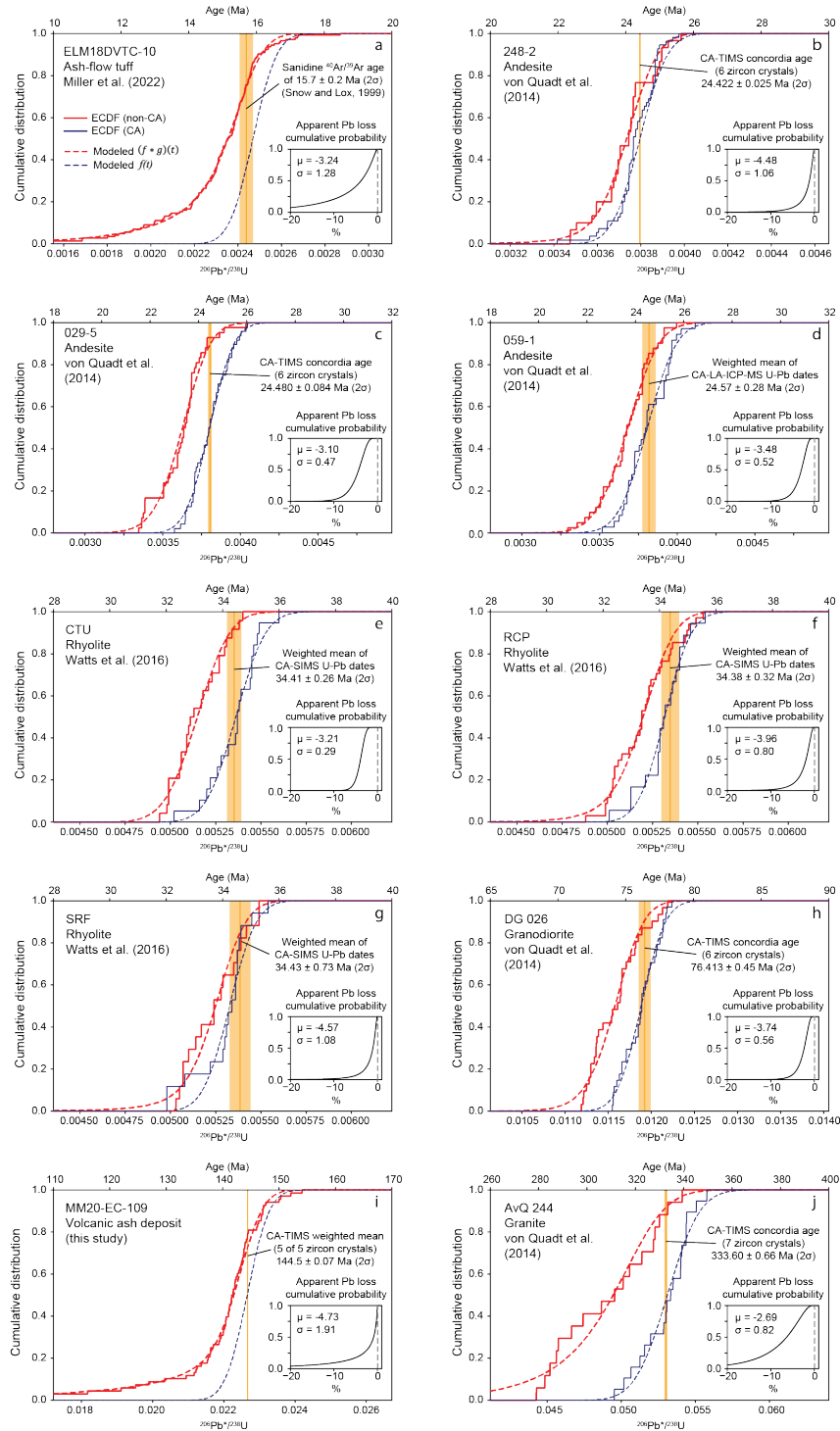


**Figure 5. Modeling of apparent Pb loss in zircon U-Pb dates acquired via LA-ICP-MS or SIMS. The best-fitting logit-normal distribution of apparent Pb loss is shown (Table 1; see Figure A1 for plots of all samples and apparent Pb loss distribution types modeled). Empirical cumulative distribution functions (ECDFs) are shown as solid lines while model results are shown as dashed lines. See text for further discussion of model results.**

97

98 scenario are  $\ll 0.05$  for all samples except SRF, suggesting that the untreated LA-ICP-MS or SIMS U-Pb dates are unlikely  
99 to have been drawn from an unperturbed U-Pb date distribution. ~~Of the continuous distributions considered, the Weibull and  
100 lognormal distributions produced the overall best fits, with average misfit values equaling 2.82 and 3.33, respectively (Fig. 4).  
101 The Pareto distribution produces a heavy tail (Fig. 3) that yielded good fits for some samples with extreme outlying values  
102 (e.g., ELM18DVTC-10 and MM20-EC-109) but poor fits for some of the other samples (average misfit of 20.1, Fig. 4). The  
103 other distribution types yielded intermediate results with average misfit values ranging between 4.8 and 8.1 (Fig. 4). With a  
104 few exceptions, p-values for both the K-S and Kuiper tests are  $> 0.05$  for the continuous distribution types we modeled (Table  
105 A1).~~

106

107

108 Figure 5 presents a comparison of actual ~~versuss~~ modeled U-Pb date distributions for each sample, with the best-fitting ~~logit-  
109 normal~~ ~~continuous apparent Pb loss~~ distribution shown (Table 1; see Figure A1 for individual plots that show the fit for each  
110 sample and distribution type). We chose to not consider discrete distributions of  ~~$g(t)$  apparent Pb loss~~ for the “best” fit because  
111 we consider it unlikely that Pb loss (or other processes that cause negative age offsets) would be limited to discrete values  
112 (e.g., Fig. 23). ~~Values of  $\mu$  for  $g(t)$  ranged from -2.69 to -4.73 with corresponding values of  $\sigma$  spanning 0.29 to 1.91. The best-  
113 fitting continuous distribution types include the gamma (ELM18DVTC-10), Weibull (248-2 and SRF), lognormal (029-5 and  
114 059-1), uniform (CTU), half normal (RCP), and Pareto (MM20-EC-109) distributions (Table 1).  $W_1$  distances ranged between  
115 ~~1.80-9~~ (sample SRF) and ~~8.17-7~~ (sample AvQ 244) and  $W_2$  distances between ~~2.90~~ and ~~11.140-34~~ (Table 1; Fig. 5). ~~In general,  
116 the Pareto, gamma, Weibull, and lognormal distributions are more likely to predict more abundant extreme values of age offset  
117 than the Rayleigh or uniform distributions (Fig. 5, Table 1, Fig. A2).~~~~

118

119

120 ~~To further examine variations in  $g(t)$  the distributions of apparent Pb loss between samples, we ~~A~~ plotted ~~plot of~~ the best-fitting  
121 ~~logit-normal~~ ~~Weibull~~ distributions (Fig. 6). ~~Even though the Weibull distribution was not the closest match for each sample,  
122 it yielded the best overall matches across samples, with misfit values  $< 10$  for all samples (Fig. 4). Figure 6 displays two distinct  
123 behaviors of  $g(t)$  (Fig. 6) apparent Pb loss when modeled using the Weibull distribution. (1) Four ~~s~~ samples with  $\mu < \sim -3$  and  $\sigma$   
124  $> 1$  and ~~Weibull shape parameter  $< 1$~~  have a  ~~$g(t)$  their~~ maximum relative probability ~~of apparent Pb loss~~ close to 0% suggesting  
125 a strongly decaying rate of age-offset (i.e., most ~~zircon experienced very little~~ Pb loss ~~perturbed U-Pb dates have very little  
126 age offset~~, while a few have more significant ~~Pb\*/U~~ offset). These samples also displayed  $W_2/W_1 \geq 1.67$ . (2) The remaining  
127 ~~six s~~ samples that yielded with  $\sigma < 1$  and generally higher  $\mu$  values ( $> -4$ ) a ~~Weibull shape parameter  $> 1$~~ , however, displayed  
128 a tendency for the mode of  ~~$g(t)$  apparent Pb loss~~ to be  $> 0\%$ , representing more of a bulk shift in age (e.g., most U-Pb dates have  
129 some ~~age~~-offset, while relatively few have very little or very much age offset). ~~These samples that~~ produced  $W_2/W_1 \leq 1.3$ .~~~~

## 30 5 Discussion

### 31 5.1 Assumptions and limitations

32 The mathematical and modeling framework that we present includes  
33 several underlying assumptions and limitations that should be  
34 considered.

35  
36 1. Because  $g(t)$  could represent any geological or analytical  
37 process that introduces negative age offsets, we use the phrase “apparent  
38 Pb loss” when describing our modeled estimates of  $g(t)$ . For instance,  
39 matrix-related systematic errors (Allen and Campbell, 2012), addition of  
40 U-Th during weathering (Pigeon et al., 2019), and even sample  
41 contamination from younger minerals could introduce negative age shifts  
42 exclusive of loss of radiogenic Pb. Common Pb corrections, particularly  
43 the  $^{207}\text{Pb}$ -correction, may also introduce a bias towards artificially low  
44  $\text{Pb}^*/\text{U}$  values (Anderson, 2002; Anderson et al., Anderson et al., 2019).  
45 We recommend that these additional complexities in the U-Pb system be  
46 considered when interpreting modeled estimates of  $g(t)$  as representing  
47 distributions of Pb loss.

48  
49 2. Our approach of parameterizing  $g(t)$  for the purpose of  
50 exploratory modeling has the advantage of yielding results that are  
51 interpretable while also being suitable for the relatively low- $n$  datasets  
52 available. However, any parametric model is likely a simplification of the  
53 true  $g(t)$ , and thus we consider our modeled estimates of  $g(t)$  to be first-order approximations. Analyzing a greater range of  
54 samples with a greater number of  $\pm\text{CA}$  *in-situ* U-Pb analyses, with ideal datasets having 100s or even 1000s of analyses per  
55 sample (e.g., Pullen et al., 2014; Sundell et al., 2021), would likely improve our ability to constrain the form(s) of  $g(t)$  and  
56 evaluate whether the logit-normal distribution or other forms of  $g(t)$  are appropriate. Such datasets would also be more  
57 amenable to nonparametric solutions of estimating  $g(t)$ .

58  
59 23. For  $g(t)$  to represent the true distribution of Pb loss, the process of convolution must be applied to  $\text{Pb}^*/\text{U}$  ratios at the  
60 time of Pb loss. Because  $\text{Pb}^*$  is progressively added to the crystal over time, a greater amount of ancient Pb loss is required to  
61 achieve the same reduction in  $\text{Pb}^*/\text{U}$  relative to recent Pb loss. This point is illustrated in Figure 1 where a 50% reduction in  
62  $\text{Pb}^*$  at 125 Myr after crystallization produces a similar reduction in  $^{206}\text{Pb}^*/^{238}\text{U}$  when compared to the same grain/zircon of the

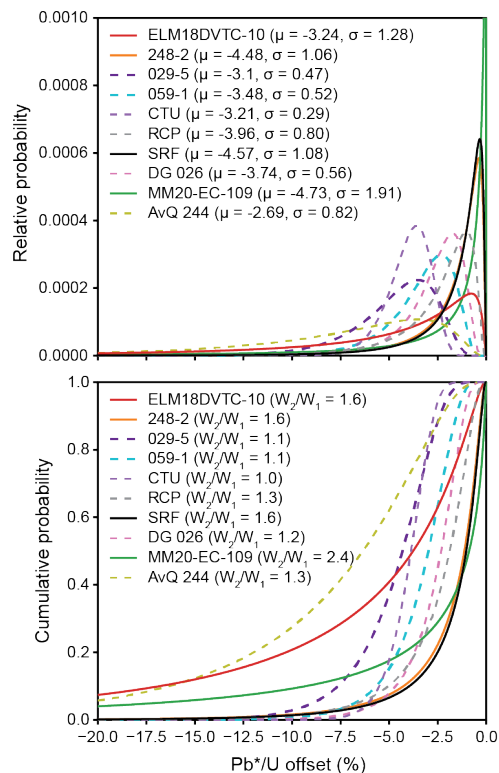


**Figure 6. Distributions of apparent Pb loss when modeled as a logit-normal distribution. Samples with  $\sigma < 1$  are shown as a dashed line.**

63 [same age](#) that lost 25% of its Pb\* at 250 Myr (present day). For this reason,  $g(t)$  can be viewed as a minimum estimate in the  
64 [case of ancient Pb loss](#). If the timing of Pb loss is known or can be estimated (e.g., [Morris et al., 2015](#)), the input Pb\*/U ratios  
65 [can be adjusted prior to analysis such that  \$g\(t\)\$  more accurately reflects the true magnitude of Pb loss](#).

66  
67 [4. The modeling framework presented above is designed for a group of cogenetic crystals with a shared crystallization](#)  
68 [age \(e.g., autocrystic zircon from the same magmatic episode; Miller et al., 2007\). This requirement stems from our definition](#)  
69 [of apparent Pb loss as a relative shift, or percentage deviation from the ~~crystallization age~~ true isotopic value \(Fig. 24\). The](#)  
70 [assumption that all zircon are coeval is a simplification, as even autocrystic zircon crystallize over a period of time, typically](#)  
71 [on  \$10^3\$ - \$10^4\$  yr timescales \(Miller et al., 2007; Rossignol et al., 2019\). Multimodal detrital samples or igneous samples with](#)  
72 [xenocrystic or inherited zircon are not easily modeled because these samples would violate our assumption of a shared](#)  
73 [crystallization age. Failure to recognize the true heterogeneity in crystallization age in such a sample could cause an incorrect](#)  
74 [interpretation of the apparent Pb loss distribution](#).

75  
76 ~~1. When modeling apparent Pb loss via convolution we make the assumption that the amount of age offset is~~  
77 ~~uncorrelated with crystallization age. We consider this to be a reasonable assumption for zircon crystals of similar age and~~  
78 ~~with a shared history (e.g., most igneous samples). However, the relative amount of Pb loss experienced by zircon of different~~  
79 ~~ages could be variable. Older zircon have experienced more radioactive decay and thus are more prone to radiation damage~~  
80 ~~(Marsellos and Garver, 2010). Similarly, some zircon incorporate elevated concentrations (>1000 ppm) of U into their crystal~~  
81 ~~structure, which promotes accelerated radiation damage and degrades the zircon matrix (White and Ireland, 2012). In~~  
82 ~~particular, Pb loss is believed to be most common at temperatures below ~250°C, at which radiation damage cannot be healed~~  
83 ~~(Schoene, 2013). Thus, detrital samples with zircon of widely varying age and provenance are more likely than igneous samples~~  
84 ~~to violate the assumption that Pb loss is independent of age. We consider some strategies for analyzing detrital zircon below~~  
85 ~~in Section 5.3.~~

86  
87 [2.5.](#) For datasets with paired non-CA and CA measurements, our modeling approach assumes that the relative precision  
88 of the analyses is similar. This is because the Gaussian distribution that best approximates the CA U-Pb date distribution,  $f(t)$ ,  
89 is convolved with the apparent Pb loss distribution  $g(t)$  to fit the non-CA U-Pb date distribution. The Watts et al. (2016) SIMS  
90 dataset shows similar relative precision regardless of treatment approach (non-CA [versus](#) CA). Some samples from the von  
91 Quadt et al. (2014) LA-ICP-MS dataset exhibit slightly lower relative precisions for non-CA versus CA, with sample AvQ  
92 244 yielding the largest difference with an average relative precision of 1.1% ( $1\sigma$ ) for non-CA dates and 0.8% ( $1\sigma$ ) for CA  
93 dates. We suggest that for the purposes of modeling apparent Pb loss, paired non-CA and CA U-Pb datasets should be collected  
94 on the same instrument using similar acquisition parameters to avoid introducing large changes in measurement precision.  
95 Alternatively, the CA U-Pb dates may be used to only constrain the  $\mu$  of  $f(t)$  in the model, with  $\sigma$  treated as an unknown  
96 parameter (e.g., for paired non-CA LA-ICP-MS and CA-ID-TIMS datasets; Figs. 5a and 5i).



97

98 ~~4. — 6. —~~ For datasets with paired non-CA and CA measurements, we do not ~~take into account~~ consider any  
99 imperfections of the chemical abrasion process. For example, although the CA treatment aims to completely remove all  
100 radiation damaged zones of the crystal (Mattinson, 2005), it is possible to have remaining residual zones of Pb loss following  
101 treatment (e.g., Schoene et al., 2010). Any such remaining compromised domains of the crystal will yield at least some apparent  
102 Pb loss when analyzed. For instance, Watts et al. (2016) interpreted three zircon U-Pb analyses from SRF to have some residual  
103 Pb loss that was not fully accounted for by the CA process (Fig. 5g). Incorporation of Pb loss-perturbed U-Pb dates when  
104 modeling  $f(t)$  would likely produce an underestimate of the true magnitude of the apparent Pb loss. ~~Additionally, the CA~~  
105 ~~process may itself damage grains to the point of being unrecoverable for future steps (e.g., mounting, analysis). Because loss~~  
106 ~~of grains via CA is likely to correlate with age, geochemistry, and/or history (e.g., older, highly metamict, or recycled grains),~~  
107 ~~there is a potential for differences between the non-CA and CA U-Pb date distributions that do not relate to apparent Pb loss.~~  
108 ~~Analyzing a dataset with a metamict-prone age fraction could result in such differences being mistakenly interpreted as the~~  
109 ~~result of apparent Pb loss if a particular group of zircon are selectively removed by CA. We suspect that this issue may be~~  
110 ~~more prevalent in detrital samples that exhibit greater diversity in zircon characteristics than in igneous samples.~~

111

112

## 113 **5.2 Distributions of apparent Pb loss**

114 What distribution type(s) characterize apparent Pb loss in natural samples? Our results strongly suggest that at least nine of the  
115 10 samples modeled have at least some systematic negative ~~age offset in~~  $^{206}\text{Pb}^*/^{238}\text{U}$  that cannot be explained by random  
116 measurement uncertainties alone. This is because the K-S and Kuiper statistical tests are unable to reject the null hypothesis  
117 for many of the apparent Pb loss distribution types considered (Table A1). For example, only the no Pb loss scenario produced  
118 a  $p$ -value  $< 0.05$  for sample MM20-EC-109, suggesting that any of the other ~~10~~ modeled distributions of apparent Pb loss may  
119 be statistically plausible for this sample. These results suggest that we cannot confidently distinguish between discrete  
120 (constant or isolated) or continuous distributions of apparent Pb loss in the datasets modeled. With the exception of Except for  
121 ELM18DVTC-10 which has 144 non-CA LA-ICP-MS analyses, the samples we analyzed have relatively low numbers of  
122 analyses (between 17 and 68, average of 32) for a given sample and treatment category (non-CA or CA) (Table 1). We  
123 ~~hypothesize suspect~~ that collection of larger- $n$  datasets would allow better ~~differentiation~~ resolution of which parameterizations  
124 of  $g(t)$  might be most appropriate ~~between possible apparent Pb loss distribution types, particularly because different~~  
125 ~~distributions can produce similarly looking functions (Fig. 3). In some cases, different distribution types can produce identical~~  
126 ~~probability density functions (e.g., the Weibull distribution interpolates between the exponential and Raleigh distributions).~~

127

128

129

30 Even if the specific distribution type(s) that characterizes *apparent Pb loss*  $g(t)$  cannot be uniquely identified, our analysis  
31 suggests two contrasting behaviors in apparent Pb loss (Fig. 6). We speculate that U-Pb dates that undergo a bulk shift (i.e.,  
32  $W_2/W_1 \cong 1$ ) may reflect a population of zircon crystals with relatively homogenous characteristics (e.g., size, U content, etc.)  
33 that have all experienced a similar post-crystallization history. Correspondingly, the population of zircon that produces U-Pb  
34 dates with a highly asymmetric distribution of age offset (i.e.,  $W_2/W_1 > \sim 1.5$ ) may reflect heterogeneity between crystals, with  
35 variable characteristics ~~and/or post-crystallization histories~~. For example, Pb loss is thought to be promoted in small zircon  
36 crystals and in zircon with elevated U (Ashwal et al., 1999; Gehrels et al., 2020), and thus distributions of particle size and/or  
37 trace element geochemistry may ~~play a role in influencing~~ influence asymmetric patterns in  $g(t)$ . Collection of size  
38 measurements and trace element concentrations from zircon in addition to measurement of the U-Pb date (e.g., Watts et al.,  
39 2016), would likely help evaluate hypotheses about the underlying factors that ~~control~~ influence such behavior of apparent Pb  
40 loss distributions. Furthermore, given the relatively small number of samples modeled in this study, we suggest that there is a  
41 need for more samples to undergo paired non-CA and CA characterization to improve understanding of the range of behaviors  
42 that may be typical. For example, it is presently unclear whether it is more common for samples to have their U-Pb dates bulk  
43 shifted (e.g., samples 029-5, 059-1, CTU, DG\_026) versus having relatively few U-Pb dates highly offset (e.g., samples MM20-  
44 EC-109 and ELM18DVTC-10; Fig. 5).

45  
46  
47 Why do some samples experience more overall apparent Pb loss than others? Although we anticipated that apparent Pb loss  
48 would be greater for older samples, our analysis shows no clear trend by sample age (although we acknowledge that the  
49 relatively high degree of apparent Pb loss modeled in the youngest sample, ELM18DVTC-10, may be a consequence of  
50 contamination from overlying units, instead of true Pb loss; Miller et al., 2022). Even the three samples from the same Eocene  
51 caldera system (CTU, RCP, and SRF) showed contrasting amounts of apparent Pb loss ( $W_2$  ranges from 2.90 to 4.42; Table 1)  
52 as noted by Watts et al. (2016). Characterizing the overall magnitude of apparent Pb loss in a wider range of samples would  
53 likely help elucidate predictive factors, if any.

### 54 ~~5.3 Detrital and other multi-modal samples~~

55 ~~The modeling framework presented above is designed for a group of cogenetic crystals with a shared crystallization age (e.g.,~~  
56 ~~autochthonous zircon from the same magmatic episode; Miller et al., 2007). This requirement stems from our definition of apparent~~  
57 ~~Pb loss as a relative shift, or percentage deviation from the crystallization age (Fig. 1). Because detrital samples are typically~~  
58 ~~multi-modal (i.e., zircon are derived from  $>1$  underlying Gaussian distribution), we cannot usually assume that the measured~~  
59 ~~U-Pb dates were all drawn from the same Gaussian distribution,  $f(t)$ . For example, volcanic arcs crystallize zircon over the~~  
60 ~~span of 10's of millions of years through multiple cycles of magmatism (Paterson and Ducea 2015). Thus, a detrital zircon age~~  
61 ~~spectra with a volcanic arc source may appear as a broad distribution of U-Pb dates that are themselves multimodal or yield~~

62 distribution tails representing waning magmatic fluxes (Caricchi et al., 2014). Failure to recognize the true heterogeneity in  
63 crystallization age in such a sample could cause an incorrect interpretation of the apparent Pb loss distribution.

64  
65 However, a sample with zircon crystals derived from multiple Gaussian distributions (e.g., detrital samples or igneous samples  
66 with antecrystic, xenocrystic, or inherited zircon; e.g., Rossignol et al., 2019) may also be modeled using this approach provided  
67 that the unperturbed U-Pb date distribution (e.g., CA-LA-ICP-MS or CA-SIMS) can be unmixed into its constituent Gaussian  
68 distributions (e.g., Sambridge and Compston, 1994). We illustrate this approach in Figure 7 where synthetic U-Pb dates are  
69 drawn from a mixture of three Gaussian distributions and convolved with the same Weibull distribution of apparent Pb loss.  
70 The resulting Pb loss-perturbed U-Pb date distribution (e.g., non-CA-LA-IC-MS or SIMS) can be produced by separately  
71 convolving each Gaussian distribution with the Pb loss distribution,  $g(t)$ , multiplying by the appropriate weighting factor, and  
72 then summing them up to unity (Fig. 7b). By modeling 1,000 synthetic U-Pb dates drawn from both the unperturbed and  
73 perturbed distributions, we found a modeled  $g(t)$  (scale = 4.6, shape = 1.3) that was a close match for the true  $g(t)$  (scale = 5,  
74 shape = 1.5) (Fig. 7c). In practice, one could apply this approach by conducting Gaussian mixture modeling on a CA-LA-ICP-  
75 MS or CA-SIMS dataset and then convolving each Gaussian separately with the apparent Pb loss distribution when minimizing  
76 the misfit.

77  
78 One word of caution with this approach is that our modeling framework assumes that the degree of age offset is independent  
79 of the age of the sample (see also point #1 in Section 5.1). To counteract this potential issue, we suggest that a U-Pb date  
80 distribution with age modes that span a significant reach of time be broken up into groups and modeled separately. In this way,  
81 the apparent Pb loss distribution that characterizes a young age mode would be allowed to vary from the apparent Pb loss  
82 distribution that has affected an older age mode.

### 83 **5.34 Importance of quantifying the distribution of apparent Pb loss in *in-situ* U-Pb geochronology**

84 The overwhelming majority of published *in-situ* U-Pb dates from zircon, minimally >600,000 and likely in the millions of  
85 analyses (Puetz et al., 2021), have not been treated using CA. In contrast, CA is now practiced routinely in the ID-TIMS  
86 community which has contributed to growing precision and accuracy over the past two decades (Schoene, 2013). However,  
87 the strategy of mitigating Pb loss through avoidance is perhaps less easily adopted to routine *in-situ* U-Pb [geochronology](#).  
88 [geochronology](#). For instance, there may be practical limitations with chemically abrading large numbers of [zircon](#)  
89 [crystalsgrains](#), including the potential loss of certain age modes that would be detrimental to provenance analysis. We thus  
90 suggest that there is a pressing need to improve quantitative characterization of apparent Pb loss distributions in non-CA *in*-  
91 *situ* U-Pb datasets to aid in interpreting these datasets and to guide strategies for future data collection.

93 It is somewhat concerning that nine of the 10 samples analyzed in this study exhibited statistically significant amounts of  
94 negative age offset from the estimated true crystallization age. Even a small age offset of a few percent, or cryptic Pb loss  
95 (Kryza et al., 2012; Watts et al., 2016), has potentially important repercussions for interpreting the age and rates of geologic  
96 events and processes. For example, there is a growing awareness in the detrital geochronological community that the youngest  
97 zircon U-Pb dates often skew unexpectedly young relative to the plausible crystallization age (e.g., Herriot et al., 2019; Gehrels  
98 et al., 2020; Schwartz et al., 2022). Presently, there is no consensus on the importance of post-depositional Pb loss on  
99 influencing depositional age interpretations (e.g., Herriott et al., 2019; Copeland, 2020; Schwartz et al., 2022). Sample MM20-  
00 EC-109 illustrates the risk well; we initially interpreted the young tail on the U-Pb date distribution to suggest a depositional  
01 age of ~125 Ma based on the youngest cluster of overlapping U-Pb dates. The youngest single analysis was a  $60.5 \pm 2.4$  Ma  
02 rim on a  $135.3 \pm 3.0$  Ma core, with the second youngest being a  $79 \pm 1.2$  Ma date measured from the core of a [grain zircon](#)  
03 [crystal](#), with the corresponding rim yielding an older  $129.8 \pm 3.6$  Ma date (Table A2). Interpretation of the youngest single U-  
04 Pb date or dates as the depositional age of this sample would have produced a highly erroneous estimate, off by up to -58% of  
05 the true eruption age of  $144.50 \pm 0.07$  ( $2\sigma$ ) Ma as determined by CA-ID-TIMS. Because this ash is interbedded within a  
06 sequence of organic rich marine mudstone in the Austral Basin of Argentina, the misinterpretation in this case could have led  
07 to an erroneous depositional age model with implications for interpreting the paleoclimatic and geodynamic context of these  
08 sediments.

09  
10 Although modeling detrital samples was outside of the scope of this study, we believe that our results bear upon maximum  
11 depositional age analysis. The tendency for the youngest U-Pb dates in a sample to be affected by Pb loss (or other similar  
12 process) complicates even conservative estimates of the maximum depositional age (Dickinson and Gehrels., 2009; Coutts et  
13 al., 2019; Schwartz et al., 2022). If apparent Pb loss follows a continuous distribution (e.g., Fig. 3d), then it is ill-advised to  
14 assume that outlying U-Pb dates may be rejected while the rest are considered unperturbed (see also discussion in Copeland,  
15 2020). Even an interpretation based on the peak age probability of the youngest age mode is likely to be too young, because  
16 the process of convolution produces a [young shift/young shift](#) in the mode of the distribution, in addition to creating a young  
17 tail (Figs. 3d; Fig. A1 and 7). Because existing methods of calculating the maximum depositional age (Dickinson and Gehrels,  
18 2009; Coutts et al., 2019; Vermeesch, 2021) ~~do not fail to~~ account for systematic negative age offsets, our analysis suggests  
19 that there is a [higher](#) probability for erroneous estimates of the maximum depositional age if (1) there are a large number of  
20 zircon crystals with crystallization ages that are close to the age of deposition, (2) the overall number of measured U-Pb  
21 analyses is very high, and/or (3) the magnitude of apparent Pb loss is high. In addition, [a heavy-tailed the distribution type of](#)  
22 [apparent Pb loss \(i.e.,  \$W\_2/W\_1 \gg 1\$ \) will result in a greater \(e.g., heavy-tailed vs not\) will also influence maximum depositional](#)  
23 [age calculations due to varying probability of finding extremely offset  \$Pb^\*/U\$  values, with samples with large  \$W\_2\$  values](#)  
24 [particularly at risk of highly inaccurate estimates.](#)

25  
26 [5.5 Strategies for future data collection](#)

27 Given the limitations of existing samples in modeling apparent Pb loss distributions, we suggest two strategies that might  
28 guide future data collection. First, increasing the number of analyses would provide improved characterization of the  
29 apparent Pb loss distribution. In particular, heavy-tailed distributions (e.g., Pareto) predict rare but highly offset values that  
30 may not be identified unless a sufficient number of grains are analyzed. **We suggest that future work focus on increasing  
31 the number of  $\pm$ CA *in situ* U-Pb analyses, with ideal datasets having 100s, or even 1000s, of analyses per sample (e.g.,  
32 Pullen et al., 2014). Such efforts are likely to be promoted by recent advances in the rate of LA-ICP-MS throughput  
33 for improved provenance characterization of detrital zircon (Sundell et al., 2021).**

34  
35 Second, increasing the precision of U-Pb date measurements will facilitate accurate identification of the apparent Pb loss  
36 distribution (Fig. 8). As the standard deviation of the unperturbed U-Pb date distribution becomes increasingly small (i.e., due  
37 to increasing analytical precision), the convolution of  $f(t)$  and  $g(t)$  will become increasingly similar to  $g(t)$  (Fig. 8). Thus, the  
38 same distribution of apparent Pb loss will be more easily discerned for higher precision U-Pb data than for lower precision  
39 data. *In situ* zircon U-Pb dates typically have 1–3% relative uncertainties (Schaltegger et al., 2015; Sharman and Malkowski,  
40 2020), similar to the ‘moderate’ precision example in Figure 8, whereas the precision achieved by CA-ID-TIMS is commonly  
41 better than 0.1% depending on U content and age of the crystal (Schaltegger et al., 2015). Thus, the ideal dataset would consist  
42 of large numbers of paired non-CA and CA-ID-TIMS measurements from randomly selected zircon from the same sample.  
43 However, given the practical limitations of cost and time involved with collecting CA-ID-TIMS measurements, we suggest  
44 that  $\pm$ CA LA-ICP-MS analysis might offer the best compromise between data quantity (i.e., rapid analysis) and precision.

45  
46 Figure 8 also illustrates the challenge of accurately identifying the distribution of apparent Pb loss when the degree of Pb  
47 loss is small in comparison to the relative precision of the U-Pb dates. For instance, a sample with low amounts of apparent  
48 Pb loss (e.g., SRF; Fig. 5) may be equally well modeled by any number of distribution types, as they all are able to collapse  
49 to  $W_1$  and  $W_2$  values approaching 0. Thus, we anticipate the ability to differentiate between apparent Pb loss distribution  
50 types to decrease as the magnitude of apparent Pb loss decreases, except for perhaps the highest resolution U-Pb datasets  
51 (e.g., ID-TIMS). However, this limitation may be partly overcome by increasing the number of analyses per sample.

## 52 6 Conclusions

53 This study presents a ~~novel~~ mathematical framework for quantifying the distribution of apparent Pb loss on U-Pb date  
54 distributions, which could include true loss of radiogenic Pb or other processes that also produce a systematically negative age  
55 offset. We show that a Pb loss-perturbed U-Pb date distribution from a set of zircon crystals with a shared crystallization age  
56 can be represented by the convolution of ~~the a~~ unperturbed Gaussian distribution that reflects measurement uncertainty in  
57 Pb\*/UU-Pb date distribution and with the a distribution that characterizes ~~of~~ Pb loss,  $g(t)$ . Our approach relies on analyzing  
58 differences between the untreated date-Pb\*/U distribution from *in-situ* U-Pb geochronology (i.e., LA-ICP-MS or SIMS) and  
59 an independent estimate of the true crystallization age, which could include U-Pb dates from a thermally annealed and

60 chemically abraded aliquot of the same sample or from another geochronometer (e.g.,  $^{40}\text{Ar}/^{39}\text{Ar}$ ). We suggest that the first and  
61 second Wasserstein distances ( $W_1$  and  $W_2$ ) of the apparent Pb loss distribution can be used to quantify the total degree of  
62 apparent Pb loss that a set of ~~grain-zircon~~ analyses has undergone, with maximum possible  $W_1$  and  $W_2$  values of 100.

63  
64 We apply this modeling framework to ten igneous samples (Miocene to Carboniferous) analyzed with LA-ICP-MS or SIMS.  
65 All but one of the samples showed a high probability that the untreated U-Pb date distribution has been perturbed by Pb loss  
66 or other equivalent process. ~~Although our analysis shows that multiple parameterizations of  $g(t)$  can achieve statistically~~  
67 ~~acceptable fits (i.e., K-S or Kuiper  $p$ -value  $>0.05$ ), we suggest that the logit-normal distribution may be a reasonable choice~~  
68 ~~for exploratory modeling of apparent Pb loss distributions. Of the eight types of continuous apparent Pb loss distributions that~~  
69 ~~we considered, the Weibull distribution produced the overall best fit.~~ However, ~~we caution that~~ the number of analyses in the  
70 samples we analyzed was generally low (17-144, average of 39); ~~future efforts to characterize  $g(t)$  may be promoted by~~  
71 ~~collection of larger- $n$  datasets and through development of nonparametric methods of estimating  $g(t)$ .~~ Furthermore, our  
72 ~~estimates of  $g(t)$  should be viewed as minimum estimates of the true amount of Pb lost, as we assumed present-day Pb loss in~~  
73 ~~our analysis. These caveats aside, which likely contributed to many of the modeled Pb loss distributions producing statistically~~  
74 ~~acceptable fits (i.e., K-S or Kuiper  $p$ -value  $>0.05$ ).~~ In general, we noted two behaviors of apparent Pb loss ~~in these samples~~;  
75 samples with a bulk shift in U-Pb date distributions ( $W_2/W_1 < \sim 1.3$ ) and samples where most ~~grains-analyses~~ had very little  
76 offset but ~~fewer grains~~ had much larger offsets ( $W_2/W_1 > \sim 1.76$ ). The overall magnitude of ~~apparent Pb loss~~  $\text{Pb}^*/\text{U}$  decrease  
77 was also found to be variable, with median values varying from -0.9% to -6.54%.

78  
79  
80 ~~Although our modeling framework is designed for analysis of cogenetic grains, and thus most appropriate for igneous samples,~~  
81 ~~we illustrate how the approach could be applied to detrital samples by first unmixing the CA U-Pb date distribution into~~  
82 ~~component Gaussian distributions. However, analysis of detrital samples with zircon of widely varying age and history may~~  
83 ~~violate an assumption of our model that the amount of apparent Pb loss is uncorrelated with age. We thus suggest that~~  
84 ~~multimodal U-Pb date distributions be divided and modeled separately to allow the apparent Pb loss distribution to vary over~~  
85 ~~time.~~

86  
87 Given the widespread application of *in-situ* U-Pb geochronology of untreated zircon across many disciplines of geosciences,  
88 improved characterization of both the distribution type(s) and magnitude of apparent Pb loss is warranted, particularly for  
89 Phanerozoic zircon where cryptic Pb loss is difficult to identify. We highlight a need for increased sampling and high- $n$   
90 characterization of paired non-CA and CA *in-situ* U-Pb datasets. ~~CA LA-ICP-MS in particular has potential given the ability~~  
91 ~~to rapidly acquire the type of large datasets that would facilitate modeling apparent Pb loss distributions.~~ In addition, we  
92 recommend simultaneous collection of parameters such as zircon size and trace elemental concentrations to aid in future efforts  
93 to understand the mechanisms of negative age offsets. Ultimately, we anticipate that improved characterization of the

94 magnitude ~~and distribution type(s)~~ of apparent Pb loss will aid in interpreting non-CA *in-situ* U-Pb datasets and guide strategies  
95 for future data collection.

## 96 **Data availability**

97 Data are archived under <https://doi.org/10.5281/zenodo.8302521> ~~<https://doi.org/10.5281/zenodo.7783226>~~. [Appendix A](#)  
98 [provides a description of exploratory modeling of different parameterizations of  \$g\(t\)\$](#) . [Figure A1 includes examples of eight](#)  
99 [continuous distribution types not explored in the main text](#). [Table A1 and Figure A2 include](#) ~~Table A1 and Figure A1 include~~  
100 summaries of all model results. [Table A2 presents a summary of model fit for each sample and distribution type considered](#).  
101 [Tables A2–A3 and A3–A4 provide U-Pb analytical results for sample MM20-EC-109 from the University of Arizona](#)  
102 [LaserChron Center \(LA-ICP-MS\) and Boise State University Isotope Geology Laboratory \(CA-ID-TIMS\), respectively](#).  
103 [Figure A2–A3 includes CL images from the University of Arizona LaserChron Center](#). [Figure A3 provides a summary of all](#)  
104 [best fitting continuous Pb loss distributions for each sample](#). [Supplemental Video 1 provides an example of convolution](#).  
105 [Supplemental Video 2 presents an exploration of the parameter space for the logit-normal distribution](#).  
106

## 107 **Code availability**

108 Code used in this research is available on GitHub ([https://github.com/grsharman/Pb\\_loss\\_modeling](https://github.com/grsharman/Pb_loss_modeling)) with the [initial-v2.0.0](#)  
109 commit archived under <https://doi.org/10.5281/zenodo.77832438302313>.  
110

## 111 **Video supplement**

112 Supplemental Video 1 is available at <https://doi.org/10.5281/zenodo.8302521> ~~<https://doi.org/10.5281/zenodo.7783226>~~. This  
113 animation provides an illustration of how a Gaussian distribution of U-Pb dates (solid, blue line),  $f(t)$ , may be perturbed by  
114 ~~exponential-logit-normal~~ Pb loss,  $g(t)$  (solid, red line). The ~~exponential~~ Pb loss distribution is first reflected about the y-axis  
115 and then iteratively shifted by small values of  $t$ ,  $g(t-\tau)$  (dashed, red line). The convolution of  $f(t)$  and  $g(t)$  at any given value of  
116  $t$  equals the summed area underneath the product of  $f(t)$  and  $g(t-\tau)$ . [Supplemental Video 2 is also available at](#)  
117 <https://doi.org/10.5281/zenodo.8302521> and [illustrates how the logit-normal distribution varies with respect to its two](#)  
118 [parameters  \$\mu\$  and  \$\sigma\$](#) . Note that we have rescaled the x-axis of the logit-normal distribution such that  $-100 < x < 0$ .  
119

## 120 **Author contribution**

121 G. Sharman and M. Malkowski co-designed the study. G. Sharman developed the code. M. Malkowski produced the U-Pb  
122 data from sample MM20-EC-109. G. Sharman and M. Malkowski wrote the manuscript.  
123

## 124 **Competing interests**

125 The authors declare that they have no conflict of interest.  
126

## 127 **Acknowledgments**

128 That authors thank Mark Pecha, George Gehrels, and staff at the University of Arizona LaserChron (supported by NSF-EAR  
129 awards #1649254 and #2050246) as well as Jim Crowley and Mark Schmitz at the Isotope Geology Laboratory at Boise State  
130 University. The project is supported in part by NSF EAR award #2243685, American Chemical Society Petroleum Research

31 Fund award #66408-DNI8, and the industrial affiliate members of the Detrital Geochronological Laboratory. We thank Kevin  
32 Befus for coding advice. [This work benefited from discussions with Alex Lipp](#) and Greg Dumond ~~for helpful discussions.~~  
33 [Comments and suggestions from two anonymous reviewers and associate editor Pieter Vermeesch resulted in substantial](#)  
34 [improvements to the manuscript.](#)

## 35 References

- 36 [Aitchison, J., and Bacon-Shone, J.: Convex linear combinations of compositions, \*Biometrika\*, 86, 351-364,](#)  
37 <https://www.jstor.org/stable/2673517>, 1999.
- 38 [Aitchison, J., and Shen, S. M.: Logistic-normal distributions: Some properties and uses, \*Biometrika\*, 67, 261-272,](#)  
39 <https://www.jstor.org/stable/2335470>, 1980.
- 40 Allen, C. M. and Campbell, I. H.: Identification and elimination of a matrix-induced systematic error in LA-ICP-MS  
41 <sup>206</sup>Pb/<sup>238</sup>U dating of zircon, *Chemical Geology*, 332, 157-165, 2012.
- 42 [Anderson, T.: Correction of common lead in U-Pb analyses that do not report <sup>204</sup>Pb, \*Chemical Geology\*, 192, 59-79, 2002.](#)  
43 [Anderson 2002, \*CG\*, v. 192, 59-79](#)
- 44 Andersen, T. and Elburg, M. A.: Open-system behaviour of detrital zircon during weathering: an example from the  
45 Palaeoproterozoic Pretoria Group, South Africa, *Geological Magazine*, 159, 561-576, 2022.
- 46 Andersen, T., Elburg, M. A. and Magwaza, B. N.: Sources of bias in detrital zircon geochronology: Discordance, concealed  
47 lead loss and common lead correction, *Earth-Science Reviews*, 197, 102899, 2019.
- 48 [Ashwal, L. D., Tucker, R. D., and Zinner, E. K.: Slow cooling of deep crustal granulites and Pb-loss in zircon, \*Geochimica et\*  
49 \[Cosmochimica Acta\]\(#\), 63, 2839-2851, 1999.](#)
- 50 Balan, E., Neuville, D. R., Trocellier, P., Fritsch, E., Muller, J. P., and Calas, G.: Metamictization and chemical durability of  
51 detrital zircon, *Am. Mineral.*, 86, 1025-1033, 2001.
- 52 Black, L. P.: Recent Pb loss in zircon: A natural or laboratory induced phenomenon?, *Chem. Geol. Isotope Geoscience section*,  
53 65, 25-33, 1987.
- 54 [Blackburn, T., Bowring, S. A., Schoene, B., Mahan, K., and Dudas, F.: U-Pb thermochronology: creating a temporal record](#)  
55 [of lithosphere thermal evolution, \*Contrib. Mineral. Petrol.\*, 162, 479-500, \[https://doi.org/10.1007/s00410-011-\]\(https://doi.org/10.1007/s00410-011-0607-6\)](#)  
56 [0607-6](#), 2011.
- 57 Bowring, S. A. and Schmitz, M. D.: High-precision U-Pb zircon geochronology and the stratigraphic record, *Rev. Mineral.*  
58 *Geochemistry*, 53, 305-326, 2003.
- 59 Burgess, S. D., Bowring, S., and Shen, S. Z.: High-precision timeline for Earth's most severe extinction, *Proc. Natl. Acad. Sci.*  
60 *U. S. A.*, 111, 3316-3321, 2014.
- 61 [Caricchi, L., Simpson, G., and Schaltegger, U.: Zircon reveals magma fluxes in the Earth's crust, \*Nature\*, 511, 457-461, 2014.](#)
- 62 Cherniak, D. J. and Watson, E. B.: Pb diffusion in zircon, *Chem. Geol.*, 172, 5-24, 2001.
- 63 Copeland, P.: On the use of geochronology of detrital grains in determining the time of deposition of clastic sedimentary strata,  
64 *Basin Research*, 32, 1532-1546, 2020.
- 65 Compston, W.: Interpretations of SHRIMP and isotope dilution zircon ages for the geological time-scale: I. The early  
66 Ordovician and late Cambrian, *Mineral. Mag.*, 64, 43-57, 2000a.
- 67 Compston, W.: Interpretation of SHRIMP and isotope dilution zircon ages for the Palaeozoic time-scale: II. Silurian to  
68 Devonian, *Mineral. Mag.*, 64, 1127-1171, 2000b.
- 69 Coutts, D. S., Matthews, W. A., and Hubbard, S. M.: Assessment of widely used methods to derive depositional ages from  
70 detrital zircon populations, *Geosci. Front.*, 34, 1421-1435, 2019.
- 71 Crowley, Q. G., Heron, K., Riggs, N., Kamber, B., Chew, D., McConnell, B., and Benn, K.: Chemical abrasion applied to LA-  
72 ICP-MS U-Pb zircon geochronology, 4, 503-518, 2014.
- 73 [Davis, D.W., Williams, I.S., and Krogh, T.E.: Historical development of zircon geochronology, \*Reviews in Mineralogy and\*  
74 \[Geochemistry, 53, 145-181, <https://doi.org/10.2113/0530145>, 2003.\]\(#\)](#)
- 75 Dickinson, W. R. and Gehrels, G. E.: Use of U-Pb ages of detrital zircons to infer maximum depositional ages of strata: A test  
76 against a Colorado Plateau Mesozoic database, *Earth Planet. Sci. Lett.*, 288, 115-125, 2009.



- 77 Froude, D. O., Ireland, T. R., Kinny, P. D., Williams, I. S., Compston, W., Williams, I. R., and Myers, J. S.: Ion microprobe  
78 identification of 4,100–4,200 Myr-old terrestrial zircons, *Nature*, 304, 616, 1983.
- 79 Geisler, T., Pidgeon, R. T., Van Bronswijk, W., and Kurtz, R.: Transport of uranium, thorium, and lead in metamict zircon  
80 under low-temperature hydrothermal conditions, *Chem. Geol.*, 191, 141–154, 2002.
- 81 Geisler, T., Pidgeon, R. T., Kurtz, R., van Bronswijk, W., and Schleicher, H.: Experimental hydrothermal alteration of partially  
82 metamict zircon, *Am. Mineral.*, 88, 1496–1513, 2003.
- 83 Gehrels, G. E.: Detrital Zircon U-Pb Geochronology Applied to Tectonics, *Annu. Rev. Earth Planet. Sci.*, 42, 127–149, 2014.
- 84 Gehrels, G., Giesler, D., Olsen, P., Kent, D., Marsh, A., Parker, W., Rasmussen, C., Mundil, R., Irmis, R., Geissman, J., and  
85 Lepre, C.: LA-ICPMS U–Pb geochronology of detrital zircon grains from the Coconino, Moenkopi, and Chinle  
86 formations in the Petrified Forest National Park (Arizona), 2, 257–282, 2020.
- 87 Gradstein, F. M., Ogg, J. G., Smith, A. G., Bleeker, W., and Lourens, L. J.: A new Geologic Time Scale, with special reference  
88 to Precambrian and Neogene, *Episodes*, 27, 83–100, 2004.
- 89 Grushka, E.: Characterization of Exponentially Modified Gaussian Peaks in Chromatography, *Anal. Chem.*, 44, 1733–1738,  
90 1972.
- 91 Herriott, T. M., Crowley, J. L., Schmitz, M. D., Wartes, M. A., and Gillis, R. J.: Exploring the law of detrital zircon: LA-ICP-  
92 MS and CA-TIMS geochronology of Jurassic forearc strata, Cook Inlet, Alaska, USA, 47, 1044-1048, 2019.
- 93 Howard, B., Sharman, G., Crowley, J. L., and Wersan, E. R.: The instrumentation dilemma: A comparison of paired LA-ICP-  
94 MS and ID-TIMS U-Pb dates from zircon, *Geological Society of America Abstracts with Programs*, 54, 2022.
- 95 Ireland, T. R. and Williams, I. S.: Considerations in zircon geochronology by SIMS, *Rev. Mineral. Geochemistry*, 53, 215–  
96 241, 2003.
- 97 Johnstone, S. A., Schwartz, T. M., and Holm-Denoma, C. S.: A Stratigraphic Approach to Inferring Depositional Ages From  
98 Detrital Geochronology Data, 7, article 57, 2019.
- 99 Kaufmann, B.: Calibrating the Devonian Time Scale: A synthesis of U-Pb ID-TIMS ages and conodont stratigraphy, *Earth-  
00 Science Rev.*, 76, 175–190, 2006.
- 01 [Kirkland, C. L., Abello, F., Danišik, M., Gardiner, N.J., and Spencer, C.: Mapping temporal and spatial patterns of zircon U-  
02 Pb disturbance: A Yilgarn Craton case study, \*Gondwana Research\*, 52, 39-47,  
03 <https://dx.doi.org/10.1016/j.gr.2017.08.004>, 2017.](#)
- 04 [Kirkland, C. L., Barnham, M., and Danišik, M.: Find a match with triple-dating: Antarctic sub-ice zircon detritus on the modern  
05 shore of Western Australia, \*Earth and Planetary Science Letters\*, 531, 115953,  
06 <https://doi.org/10.1016/j.epsl.2019.115953>, 2020.](#)
- 07 [Kirkland et al., 2017, GR, v. 52, 39-47](#)
- 08 [Kirkland et al., 2020, GR, v. 77, 223-237](#)
- 09 Kröner, A., Jaekel, P., and Williams, I. S.: Pb-loss patterns in zircons from a high-grade metamorphic terrain as revealed by  
10 different dating methods: U-Pb and Pb-Pb ages for igneous and metamorphic zircons from northern Sri Lanka,  
11 *Precambrian Res.*, 66, 151–181, 1994.
- 12 Kryza, R., Crowley, Q. G., Larionov, A., Pin, C., Oberc-Dziedzic, T., and Mochnacka, K.: Chemical abrasion applied to  
13 SHRIMP zircon geochronology: An example from the Variscan Karkonosze Granite (Sudetes, SW Poland),  
14 *Gondwana Res.*, 21, 757–767, 2012.
- 15 Lipp, A.G., and Vermeesch, P.: [Short communication: The Wasserstein distance as a dissimilarity metric for comparing detrital  
16 age spectra and other geological distributions](#) [Comparing detrital age spectra, and other geological distributions, using  
17 the Wasserstein distance, \*Earth ArXiv preprint\*, <https://doi.org/10.31223/X5TM02> \*Geochronology\*, 5, 263-270,  
18 <https://doi.org/10.5194/gchron-5-263-2023>, 2023.](#)
- 19 Marsellos, A. E. and Garver, J. I.: Radiation damage and uranium concentration in zircon as assessed by Raman spectroscopy  
20 and neutron irradiation, *Am. Mineral.*, 95, 1192–1201, 2010.
- 21 Mattinson, J. M.: Zircon U-Pb chemical abrasion (“CA-TIMS”) method: Combined annealing and multi-step partial  
22 dissolution analysis for improved precision and accuracy of zircon ages, *Chem. Geol.*, 220, 47–66, 2005.
- 23 [Mead, R.: A generalized logit-normal distribution, \*Biometrics\*, 21, 721-732, <https://www.jstor.org/stable/2528553>,  
24 1965.](#)
- 25 Mezger, K. and Krogstad, J. E.: Interpretation of discordant U-Pb zircon ages: An evaluation, *J. Metamorph. Geol.*, 15, 127–  
26 140, 1997.

- 27 Miller, J. S., Matzel, J. E. P., Miller, C. F., Burgess, S. D., and Miller, R. B.: Zircon growth and recycling during the assembly  
28 of large, composite arc plutons, *J. Volcanol. Geotherm. Res.*, 167, 282–299, 2007.
- 29 Miller, E. L., Raftrey, M. E., and Lund Snee, J.-E.: Downhill from Austin and Ely to Las Vegas: U-Pb detrital zircon suites  
30 from the Eocene–Oligocene Titus Canyon Formation and associated strata, Death Valley, California, *Geol. Soc. Am.*  
31 *Spec. Pap.*, 555, 359–378, 2022.
- 32 Morris, G. A., Kirkland, C. L., and Pease, V.: Orogenic paleofluid flow recorded by discordant detrital zircons in the  
33 Caledonian foreland basin of northern Greenland, 7, 138–143, 2015.
- 34 Nasdala, L., Hanchar, J. M., Kronz, A., and Whitehouse, M. J.: Long-term stability of alpha particle damage in natural zircon,  
35 *Chem. Geol.*, 220, 83–103, 2005.
- 36 [Olierook et al., 2021, GR, v. 92, 102–112.](#)
- 37 Orejana, D., Merino Martínez, E., Villaseca, C., and Andersen, T.: Ediacaran–Cambrian paleogeography and geodynamic  
38 setting of the Central Iberian Zone: Constraints from coupled U-Pb–Hf isotopes of detrital zircons, *Precambrian Res.*,  
39 261, 234–251, 2015.
- 40 [Pidgeon, R. T., O’Neil, J. R., and Silver, L. T.: Uranium and lead isotopic stability in metamict zircon under experimental  
41 hydrothermal conditions. \*Science\*, 154, 1538–1540. <https://www.jstor.org/stable/1720453>, 1966.](#)
- 42 [Paterson, S. R. and Ducea, M. N.: Are magmatic tempos: Gathering the evidence, 11, 91–98, 2015.](#)
- 43 Pidgeon, R. T., Nemchin, A. A., and Whitehouse, M. J.: The effect of weathering on U–Th–Pb and oxygen isotope systems of  
44 ancient zircons from the Jack Hills, Western Australia, *Geochim. Cosmochim. Acta*, 197, 142–166, 2017.
- 45 Pidgeon, R. T., Nemchin, A. A., Roberts, M. P., Whitehouse, M. J., and Bellucci, J. J.: The accumulation of non-formula  
46 elements in zircons during weathering: Ancient zircons from the Jack Hills, Western Australia, *Chem. Geol.*, 530,  
47 119310, <https://doi.org/10.1016/j.chemgeo.2019.119310>, 2019.
- 48 Press, W. H., Teukolsky, S. A., Vetterling, W. T., and Flannery, B. P.: Numerical Recipes: The Art of Scientific Computing,  
49 3rd Editio., Cambridge University Press, 1235 pp., 2007.
- 50 Puetz, S. J., Spencer, C. J., and Ganade, C. E.: Analyses from a validated global U–Pb detrital zircon database: Enhanced  
51 methods for filtering discordant U–Pb zircon analyses and optimizing crystallization age estimates, *Earth-Science*  
52 *Rev.*, 220, 103745, <https://doi.org/10.1016/j.earscirev.2021.103745>, 2021.
- 53 Pullen, A., Ibáñez-Mejía, M., Gehrels, G. E., Ibáñez-Mejía, J. C., and Pecha, M.: What happens when  $n=1000$ ? Creating large-  
54  $n$  geochronological datasets with LA-ICP-MS for geologic investigations, *J. Anal. At. Spectrom.*, 29, 971–980, 2014.
- 55 Reimink, J. R., Davies, J. H. F. L., Waldron, J. W. F., and Rojas, X.: Dealing with discordance: A novel approach for analysing  
56 U–Pb detrital zircon datasets, *J. Geol. Soc. London.*, 173, 577–585, 2016.
- 57 Rioux, M., Bowring, S., Kelemen, P., Gordon, S., Dudás, F., and Miller, R.: Rapid crustal accretion and magma assimilation  
58 in the Oman–U.A.E. ophiolite: High precision U–Pb zircon geochronology of the gabbroic crust, *J. Geophys. Res.*  
59 *Solid Earth*, 117, 2012.
- 60 Rossignol, C., Hallot, E., Bourquin, S., Poujol, M., Jolivet, M., Pellenard, P., Ducassou, C., Nalpas, T., Heilbronn, G., Yu, J.,  
61 and Dabard, M. P.: Using volcanoclastic rocks to constrain sedimentation ages: To what extent are volcanism and  
62 sedimentation synchronous?, *Sediment. Geol.*, 381, 46–64, 2019.
- 63 Ruiz, M., Schaltegger, U., Gaynor, S. P., Chiaradia, M., Abrecht, J., Gislser, C., Giovanoli, F., and Wiederkehr, M.: Reassessing  
64 the intrusive tempo and magma genesis of the late Variscan Aar batholith: U–Pb geochronology, trace element and  
65 initial Hf isotope composition of zircon, *Swiss J. Geosci.*, 115, 1–24, 2022.
- 66 [Sambridge, M. S. and Compston, W.: Mixture modeling of multi-component data sets with application to ion-probe zircon  
67 ages. \*Earth Planet. Sci. Lett.\*, 128, 373–390. \[https://doi.org/10.1016/0012-821X\\(94\\)90157-0\]\(https://doi.org/10.1016/0012-821X\(94\)90157-0\), 1994.](#)
- 68 Saylor, J. E. and Sundell, K. E.: Quantifying comparison of large detrital geochronology data sets, 12, 203–220,  
69 <https://doi.org/10.1130/GES01237.1>, 2016.
- 70 [Schaltegger, U., Schmitt, A. K., and Horstwood, M. S. A.: U–Th–Pb zircon geochronology by ID-TIMS, SIMS, and laser  
71 ablation ICP-MS: Recipes, interpretations, and opportunities. \*Chem. Geol.\*, 402, 89–110, 2015.](#)
- 72 Schoene, B., Guex, J., Bartolini, A., Schaltegger, U., and Blackburn, T. J.: Correlating the end-Triassic mass extinction and  
73 flood basalt volcanism at the 100 ka level, *Geology*, 38, 387–390, <https://doi.org/10.1130/G30683.1>, 2010.
- 74 Schoene, B., Schaltegger, U., Brack, P., Latkoczy, C., Stracke, A., and Günther, D.: Rates of magma differentiation and  
75 emplacement in a ballooning pluton recorded by U–Pb TIMS-TEA, Adamello batholith, Italy, *Earth Planet. Sci. Lett.*,  
76 355–356, 162–173, 2012.

77 Schoene, B.: U-Th-Pb Geochronology, Treatise on Geochemistry (Second Edition), 4, 341–378, 2013.

78 ~~Schoene, B., Samperton, K. M., Eddy, M. P., Keller, G., Adatte, T., Bowring, S. A., Khadri, S. F. R., and Gertsch, B.: U-Pb~~  
79 ~~geochronology of the Deccan Traps and relation to the end-Cretaceous mass extinction, Science, 347, 182–184, 2015.~~

80 ~~Schoene, B., Eddy, M. P., Samperton, K. M., Keller, C. B., Keller, G., Adatte, T., and Khadri, S. F. R.: U-Pb constraints on~~  
81 ~~pulsed eruption of the Deccan Traps across the end-Cretaceous mass extinction, Science (80 -), 363, 862–866, 2019.~~

82 Schwartz, T. M., Souders, A. K., Lundstern, J.-E., Gilmer, A. K., and Thompson, R. A.: Revised age and regional correlations  
83 of Cenozoic strata on Bat Mountain, Death Valley region, California, USA, from zircon U-Pb geochronology of  
84 sandstones and ash-fall tuffs, Geosphere, 19, 235–257, 2022.

85 ~~Sharman, G. R., Covault, J. A., Flaig, P. P., Dunn, R., Füsse-Durham, P., Larson, T. E., Shanahan, T. M., Dubois, K., Shaw,~~  
86 ~~J. B., Crowley, J. L., Shaulis, B.: Coastal response to global warming during the Paleocene-Eocene Thermal Maximum,~~  
87 ~~625, 111664, <https://doi.org/10.1016/j.palaco.2023.111664>, 2023.~~

88 ~~Sharman, G. R. and Malkowski, M. A.: Needles in a haystack: Detrital zircon U-Pb ages and the maximum depositional age~~  
89 ~~of modern global sediment, Earth-Science Rev., 203, 103109, 2020.~~

90 Silver, L. T. and Deutsch, S.: Uranium-Lead Isotopic Variations in Zircons: A Case Study, J. Geol., 71, 721–758, 1963.

91 Snow, J. K. and Lux, D. R.: Tectono-sequence stratigraphy of Tertiary rocks in the Cottonwood Mountains and northern Death  
92 Valley area, California and Nevada, Geol. Soc. Am. Spec. Pap., 333, 17–64, 1999.

93 Solari, L. A., Ortega-Obregón, C., and Bernal, J. P.: U-Pb zircon geochronology by LAICPMS combined with thermal  
94 annealing: Achievements in precision and accuracy on dating standard and unknown samples, Chem. Geol., 414,  
95 2015.

96 Spencer, C. J., Kirkland, C. L., and Taylor, R. J. M.: Strategies towards statistically robust interpretations of in situ U-Pb zircon  
97 geochronology, Geosci. Front., 7, 581–589, 2016.

98 Stern, T. W., Goldich, S. S., and Newell, M. F.: Effects of weathering on the U-Pb ages of zircon from the Morton Gneiss,  
99 Minnesota, Earth Planet. Sci. Lett., 1, 369–371, 1966.

00 Sundell, K. E., Gehrels, G. E., and Pecha, M. E.: Rapid U-Pb Geochronology by Laser Ablation Multi-Collector ICP-MS,  
01 Geostand. Geoanalytical Res., 45, 37–57, 2021.

02 Tilton, G. R., Patterson, C., Brown, H., Ingham, M., Hayden, R., Hess, D., and Larsen, E., J.: Isotopic composition and  
03 distribution of lead, uranium, and thorium in a Precambrian granite, Bull. Geol. Soc. Am., 66, 1131–1148, 1955.

04 Ver Hoeve, T. J., Scoates, J. S., Wall, C. J., Weis, D., and Amini, M.: Evaluating downhole fractionation corrections in LA-  
05 ICP-MS U-Pb zircon geochronology, Chem. Geol., 483, 201–217, 2018.

06 Vermeesch, P.: Dissimilarity measures in detrital geochronology, Earth-Science Rev., 178, 310–321, 2018a.

07 ~~Vermeesch, P.: Statistical models for point-counting data, Earth-Science Rev., 501, 112–118, 2018b.~~

08 Vermeesch, P.: Maximum depositional age estimation revisited, Geosci. Front., 12, 843–850, 2021.

09 ~~Virtanen, P., Gommers, R., Oliphant, T. E., Haberland, M., Reddy, T., Cournapeau, D., Burovski, E., Peterson, P., Weckesser,~~  
10 ~~W., Bright, J., van der Walt, S. J., Brett, M., Wilson, J., Millman, K. J., Mayorov, N., Nelson, A. R. J., Jones, E.,~~  
11 ~~Kern, R., Larson, E., Carey, C. J., Polat, I., Feng, Y., Moore, E. W., VanderPlas, J., Laxalde, D., Perktold, J.,~~  
12 ~~Cimrman, R., Henriksen, I., Quintero, E. A., Harris, C. R., Archibald, A. M., Ribeiro, A. H., Pedregosa, F., van~~  
13 ~~Mulbregt, P., Vijaykumar, A., Bardelli, A. Pietro, Rothberg, A., Hilboll, A., Kloeckner, A., Scopatz, A., Lee, A.,~~  
14 ~~Rokem, A., Woods, C. N., Fulton, C., Masson, C., Häggström, C., Fitzgerald, C., Nicholson, D. A., Hagen, D. R.,~~  
15 ~~Pasechnik, D. V., Olivetti, E., Martin, E., Wieser, E., Silva, F., Lenders, F., Wilhelm, F., Young, G., Price, G. A.,~~  
16 ~~Ingold, G. L., Allen, G. E., Lee, G. R., Audren, H., Probst, I., Dietrich, J. P., Silterra, J., Webber, J. T., Slavič, J.,~~  
17 ~~Nothman, J., Buehner, J., Kuliek, J., Schönberger, J. L., de Miranda Cardoso, J. V., Reimer, J., Harrington, J.,~~  
18 ~~Rodríguez, J. L. C., Nunez-Iglesias, J., Kuczynski, J., Tritz, K., Thoma, M., Newville, M., Kümmerer, M.,~~  
19 ~~Bölingbroke, M., Tartre, M., Pak, M., Smith, N. J., Nowaczyk, N., Shebanov, N., Pavlyk, O., Brodtkorb, P. A., Lee,~~  
20 ~~P., McGibbon, R. T., Feldbauer, R., Lewis, S., Tygier, S., Sievert, S., Vigna, S., Peterson, S., More, S., Pudlik, T., et~~  
21 ~~al.: SciPy 1.0: fundamental algorithms for scientific computing in Python, Nat. Methods, 17, 261–272,~~  
22 ~~<https://doi.org/10.1038/s41592-019-0686-2>, 2020.~~

23 von Quadt, A., Gallhofer, D., Guillong, M., Peytcheva, I., Waelle, M., and Sakata, S.: U-Pb dating of CA/non-CA treated  
24 zircons obtained by LA-ICP-MS and CA-TIMS techniques: Impact for their geological interpretation, J. Anal. At.  
25 Spectrom., 29, 1618–1629, 2014.

- 26 Watts, K. E., Coble, M. A., Vazquez, J. A., Henry, C. D., Colgan, J. P. and John, D. A.: Chemical abrasion-SIMS (CA-SIMS)  
27 U-Pb dating of zircon from the late Eocene Caetano caldera, Nevada *Chemical Geology*, 439, 139-151, 2016.
- 28 Wetherill, G. W.: Discordant Uranium-Lead Ages, 1, *Trans. Am. Geophys. Union*, 37, 320–326, 1956.
- 29 ~~White, L. T. and Ireland, T. R.: High uranium matrix effect in zircon and its implications for SHRIMP U-Pb age~~  
30 ~~determinations, *Chem. Geol.*, 306–307, 78–91, 2012.~~
- 31 Willner, A. P., Sindern, S., Metzger, R., Ermolaeva, T., Kramm, U., Puchkov, V., and Kronz, A.: Typology and single grain  
32 U/Pb ages of detrital zircons from Proterozoic sandstones in the SW Urals (Russia): Early time marks at the eastern  
33 margin of Baltica, *Precambrian Res.*, 124, 1–20, 2003.
- 34 Zeh, A., Wilson, A. H., and Ovtcharova, M.: Source and age of upper Transvaal Supergroup, South Africa: Age-Hf isotope  
35 record of zircons in Magaliesberg quartzite and Dullstroom lava, and implications for Paleoproterozoic (2.5-2.0 Ga)  
36 continent reconstruction, *Precambrian Res.*, 278, 1–21, 2016.